July 2023

ELECTRICAL RESISTIVITY MAPPING OF LOWER RIO GRANDE RIVER-GROUNDWATER INTERACTIONS

NM WRRI Technical Completion Report No. 405

Autumn Joy Pearson
Kenneth C. Carroll
Dale F. Rucker
Chia-Hsing Tsai
Erek H. Fuchs

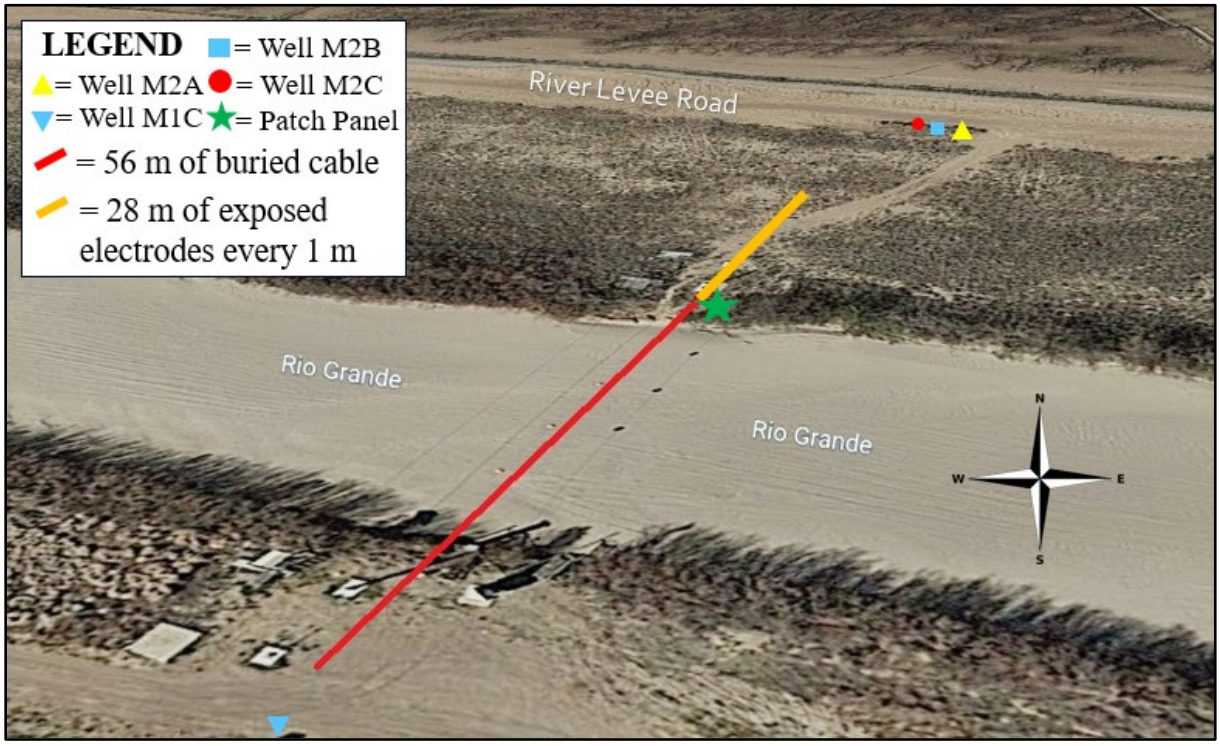

Study area site in the Lower Rio Grande in Mesquite, New Mexico.

New Mexico Water Resources Research Institute
New Mexico State University
MSC 3167, P.O. Box 30001
Las Cruces, New Mexico 88003-0001
(575) 646-4337 email: nmwrri@nmsu.edu

ELECTRICAL RESISTIVITY MAPPING OF LOWER RIO GRANDE RIVER-GROUNDWATER INTERACTIONS

By

Autumn Joy Pearson, Kenneth C. Carroll, Dale F. Rucker, Chia-Hsing Tsai
Department of Plant and Environmental Science, New Mexico State University

Erek H. Fuchs
Elephant Butte Irrigation District

TECHNICAL COMPLETION REPORT
Account Number 132070
Technical Completion Report #405

July 2023

New Mexico Water Resources Research Institute
In cooperation with
Department of Plant and Environmental Science
New Mexico State University
and
Elephant Butte Irrigation District

The research on which this report is based was financed in part by the Elephant Butte Irrigation District, The New Mexico State University, and by the U.S. Department of the Interior, Geological Survey, through the New Mexico Water Resources Research Institute. This material is based upon work supported by the U.S. Geological Survey under Grant/Cooperative Agreement No. (G16AP00072).

Page Intentionally Left Blank

DISCLAIMER

The purpose of the NM Water Resources Research Institute (NM WRRI) technical reports is to provide a timely outlet for research results obtained on projects supported in whole or in part by the institute. Through these reports the NM WRRI promotes the free exchange of information and ideas and hopes to stimulate thoughtful discussions and actions that may lead to resolution of water problems. The NM WRRI, through peer review of draft reports, attempts to substantiate the accuracy of information contained within its reports, but the views and conclusions contained in this document are those of the authors and should not be interpreted as representing the opinions or policies of the U.S. Geological Survey. Mention of trade names or commercial products does not constitute their endorsement by the U.S. Geological Survey.

ABSTRACT

In the current era of rapid environmental changes, more rivers are projected to dry up and transition to disconnected systems in unprecedented duration and frequency. However, surface-groundwater interactions including connectivity remain a challenge to characterize, especially for managed-ephemeral rivers such as the lower Rio Grande in southern New Mexico where conjunctive use for irrigated agriculture is prevalent. This investigation used a noninvasive and spatially distributed geophysical method (i.e., time-lapse electrical resistivity) for mapping the water table below and adjacent to the Rio Grande, which has been validated using groundwater table and conductivity monitoring well data. Time-lapse monitoring of electrical resistivity (inversely related to electrical conductivity and also water saturation) before, during, and after the irrigation season has been used to characterize the transient and spatial connectivity of the water table with the base of the Rio Grande from disconnection, to connection, and back to disconnection. The relationships between electrical conductivity from the geophysical analysis versus the large array of ancillary data helped to narrow down the driver of observed temporal changes in connectivity after the transition from disconnection to connection. Results have shown resistivity impacts due primarily to variations in water saturation during Rio Grande water arrival, and some influence after water arrival from water temperature and aqueous electrical conductivity (i.e., salinity) differences between resident groundwater and the infiltrating surface water. The relationships between bulk conductivity versus aqueous salinity and water saturation have been developed using laboratory experiments and correlation coefficient analysis to evaluate the time-lapse resistivity data, the characterization of surface-groundwater connectivity, and the transition from losing to gaining stream. The surface water temperature showed a direct and strong correlation to the electrical conductivity of shallow sediments, which was similar to the river stage/groundwater elevation drivers of infiltration. This type of spatiotemporal groundwater level assessment advances our disconnection process characterization capabilities, and will support the sustainable conjunctive use of surface water and groundwater especially for non-perennial systems.

Keywords: Rio Grande; electrical resistivity; ephemeral; non-perennial; surface water disconnection.

ACKNOWLEDGMENTS

This study was supported financially by Elephant Butte Irrigation District (EBID), New Mexico State University, and the U.S. Department of the Interior, Geological Survey through the New Mexico Water Resources Research Institute. We are very grateful for the technical support provided by Delbert Humberson and other employees of the International Boundary & Water Commission. We thank EBID for their financial support, sharing of data, invaluable expertise, and assistance with data acquisition. We thank Dr. Ahmed Elaksher, Dr. Naima Khan, Dr. Ruba Mohamed, Michael Hitzelberger, Tanzila Ahmed, and Cheyenne Stice for their help with equipment installation and support with data collection.

TABLE OF CONTENTS

LIST OF TABLES

LIST OF FIGURES

Page Intentionally Left Blank

INTRODUCTION

River-groundwater interactions are often ignored in hydrologic measurement (Winter et al., 1998), even though they are critical for understanding issues of water quality and quantity (Ikard et al., 2021; Brunner et al., 2017; Harvey and Gooseff, 2015; Banks et al., 2011; Findlay, 1995). This is because the spatial distribution of infiltration/seepage through a surface water source is known to depend on the state of connection (Brunner et al., 2009), which can be paramount to understanding biogeochemical cycling of nutrients and pollutants within the hyporheic zone (Krause et al., 2011; Zhou et al., 2014; Shabaga and Hill, 2010; Findlay, 1995).

Some rivers oscillate between a gaining or losing system (Wroblicky et al., 1998), and a single stream can be comprised of both gaining and losing stretches. A system is said to be connected when the area beneath a riverbed is fully saturated with groundwater, and disconnected when river-groundwater are separated by an unsaturated portion of soil or other divider. The differentiation and transition between these two cases depend on the hydraulic head of both river and groundwater which drives the hydraulic gradient direction.

When predicting the impacts of groundwater development on surface water resources, river-groundwater in gaining systems are typically assumed to be fully connected, and conversely, losing systems are also typically assumed to be fully connected (Brunner et al., 2011). This over-simplification of riverbed heterogeneity can amount to significant error in water volume quantification over long river reaches (Irvine, et al., 2012; Singha et al., 2008).

As illustrated in Figure 1, models have been developed to show the possibility of partial connection/disconnection between river and groundwater, where the connected part of the river and the groundwater below would be spatially variable due to groundwater mounding, local

recharge, riverbed conformation, or other factors. The specific location and magnitude of partial connection of stretches of water are often unknown.

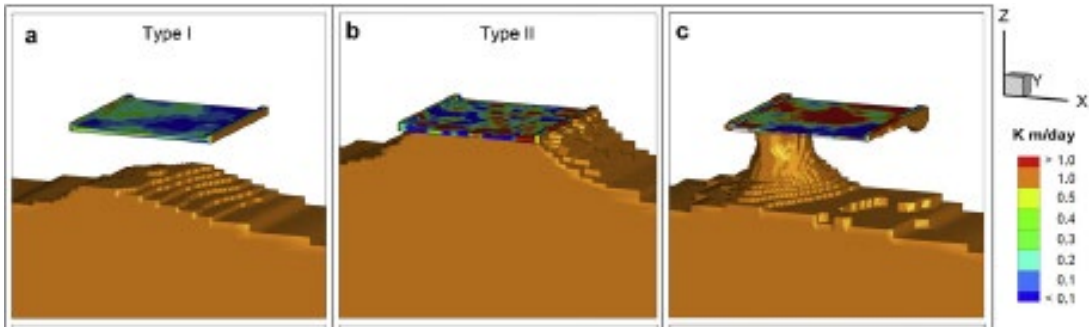

Figure 1. Model renditions of (a) Complete Disconnection, (b) Complete Connection, and (c) Partial Disconnection (Irvine et al., 2012).

The above discussion affirms the need for improved techniques to quantify river-groundwater connection with spatial and temporal complexities (Brunner, 2011; Sophocleous, 2002). However, the geological, hydrological, and biogeochemical heterogeneity in the surface-ground water interface makes it difficult to characterize with only direct observation techniques, which are generally spatially discontinuous and data limited (McLachlan et al., 2017).

Geophysics encapsulates noninvasive, indirect methods of investigating the subsurface and has been increasingly used to identify spatial and temporal variability throughout the earth. With supporting ground-truthing or validation data, geophysics is an effective tool for characterizing numerous properties and parameters (Crook et al., 2008; McLachlan et al., 2017). The use of geophysical methods has an advantage over other methods for mapping partial disconnection: it offers large-scale spatially distributed imaging, is noninvasive, and is able to image the subsurface from the surface (Rucker, 2010), unlike piezometer drilling, groundwater well installation, and other direct observation techniques that may be limited by environmental protection or unfavorable site conditions (McLachlan et al., 2017). In particular, electrical

resistivity tomography (ERT) is a promising geophysical method that can be used for mapping surface-groundwater exchange (Acworth et al., 2003; Mansoor and Slater, 2007; Nyquist et al., 2008; Singha et al., 2008).

ERT involves the application of an electrical current through the subsurface in order to determine the distribution of electrical resistivity in a 2D plot of resistivity (Ω·m) vs. depth (m). Resistivity values are related to other variables such as water and soil electrical conductivity (EC), soil type, soil mineral composition, water salinity, water total dissolved solids (TDS), temperature, and water saturation. Therefore, one can garner various information of interest by using ERT to study the subsurface. Water saturation specifically can be derived by converting the resistivity data to EC (by taking the mathematical inverse) and then using Archie's Law (Archie, 1942) to relate EC to water saturation. Time-lapse ERT has been successfully used many times to study the relationship between resistivity and hyporheic exchange using these concepts (Ward et al., 2010; Clémence et al., 2017), as well as river stage (Johnson et al., 2012). Studying this relationship is valuable, because the subsurface is a heterogeneous combination of differing materials that naturally have different "resistivity footprints" due to their chemical composition and properties of the fluids in their pores. The general principles behind this method (i.e., varied electrical response between separate materials) have been known for a long time.

There is generally a lack of information on the quantitative hydrology pertaining to differently connected stream systems. Often, even when a state of connection or disconnection between surface and groundwater is known, the temporal and spatial distribution of said connection and disconnection is still unknown. Clearly, there are large gaps in knowledge in a subject where a deeper understanding would likely be very helpful for sustainable river management (Harvey and Gooseff, 2015; Ward, 2016).

The objective of this investigation was to use time-lapse ERT over a period of one year along a portion of the lower Rio Grande in southern New Mexico in order to investigate temporal and spatial river-groundwater connectivity throughout the 2020 irrigation season.

METHODS AND MATERIALS

2.1 Site Description

Time-lapse ERT was utilized over a reach of the lower Rio Grande that flows north to south down the United States and across the border into Mexico, following the Rio Grande rift. The lower Rio Grande is part of, and recharges into, the Mesilla Basin/Conejos-Médanos (Mesilla Basin) aquifer system, and is under the management of the International Boundary and Water Commission (IBWC) and operated by the US Bureau of Reclamation as the Rio Grande Project. The New Mexico portion of the Rio Grande Project features the Elephant Butte Irrigation District (EBID), which is the largest irrigated agricultural producer in the region (Fuchs et al., 2019). This aquifer system is the main source of water for agricultural, industrial, and municipal use in El Paso, Texas, Las Cruces, New Mexico, and Ciudad Juárez, Chihuahua, Mexico, and is at the center of ongoing litigation among between New Mexico, Texas, and the United States.

The particular cross-section of the Rio Grande studied in this project is outside of Mesquite, New Mexico (seen in Figure 2), and downstream from the Mesilla, Caballo, and Elephant Butte Dams as well as the city of Las Cruces, New Mexico.

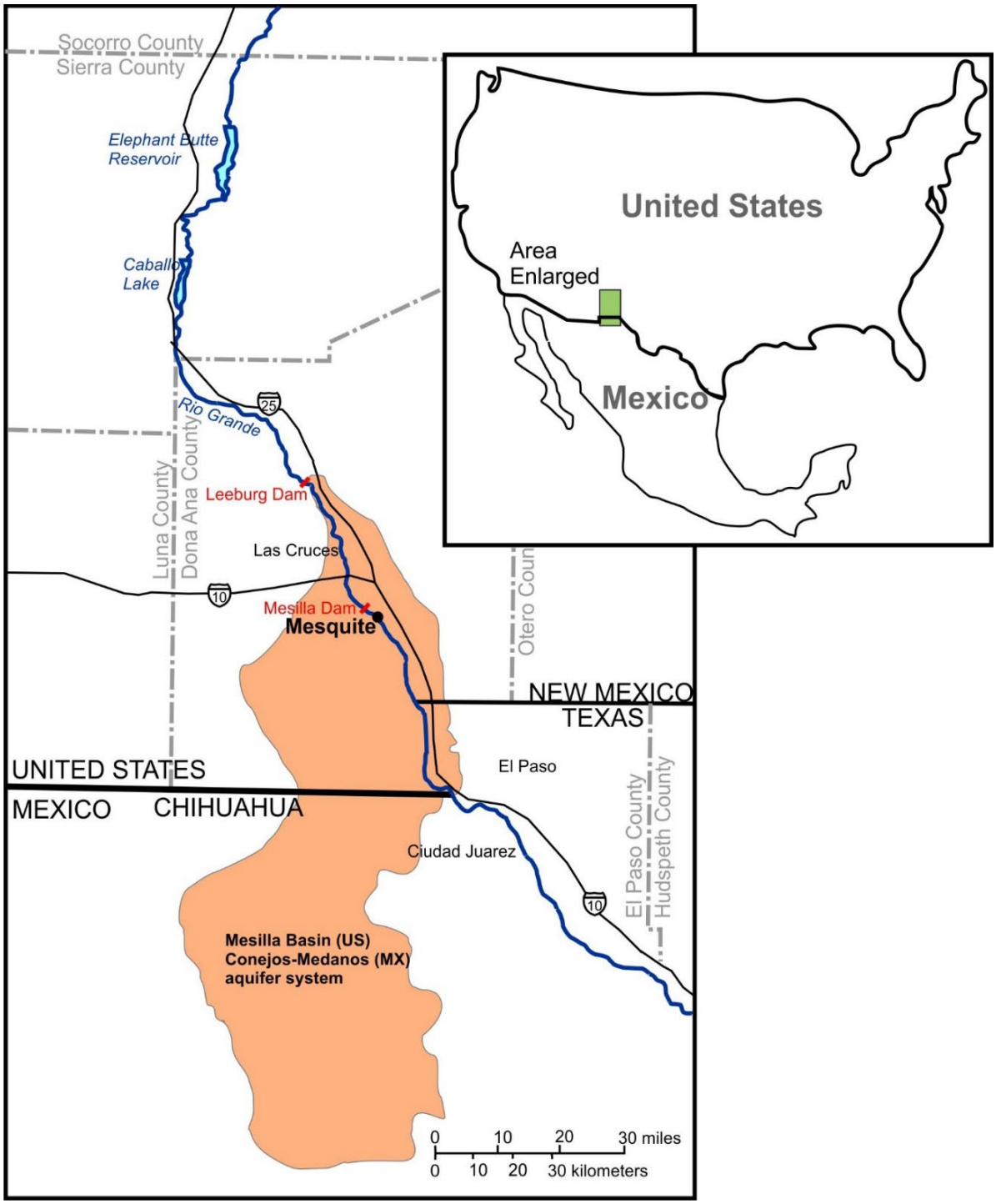

Figure 2. Location of the Mesilla Basin with Mesquite study site delineated (adapted from Teeple, 2017).

Using field observations at the catchment scale, it has been shown that portions of the lower Rio Grande transition from gaining to losing, while some sections transition from losing to

completely disconnected (Fuchs et al., 2019), making it an ideal area to observe river-groundwater connection transitions. There are pecan orchards that utilize flood irrigation on both sides of the river site, using surface water and groundwater conjunctively and differently throughout the irrigation season. Local protracted drought over the last decade or so has prompted a greater dependence on groundwater resources in order to meet crop requirements, further justifying the use of ERT in this area (see Figure 3 study area).

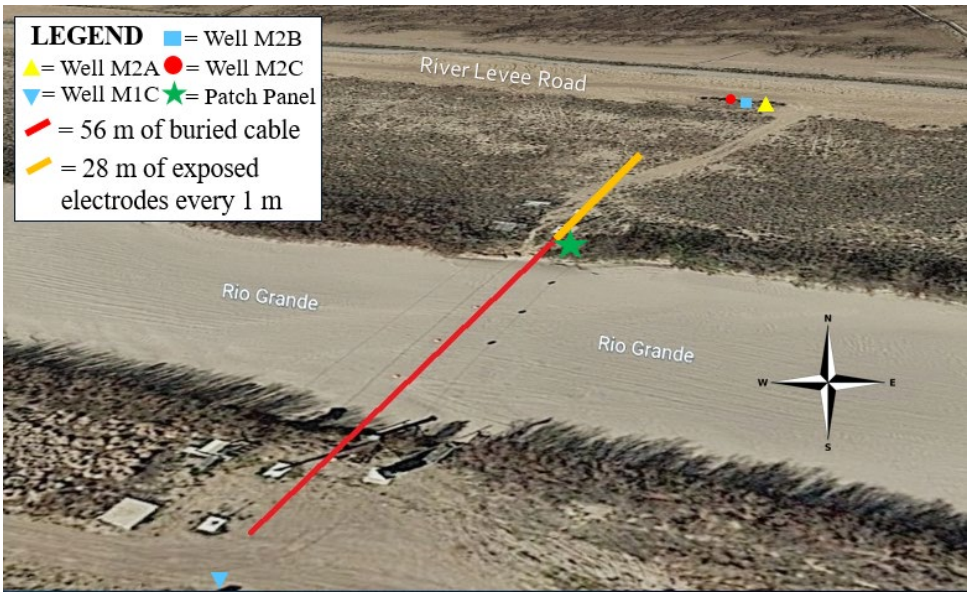

Figure 3. Photo and diagram of the study area site in the Lower Rio Grande in Mesquite, NM.

Flow in this portion of the river is ephemeral. In most of the past two decades there has been little or no flow for at least half of the year, and then moderate flow during irrigation season (i.e., generally summer time), which is entirely controlled by release of water from the Elephant Butte Dam, Caballo Dam, and the diversion at Mesilla Dam. The fact that there is essentially no flow except during dam release times confirms that this stretch of the lower Rio Grande is a losing stream, because there is no baseflow discharged from groundwater into the Rio Grande. However, the sustained dam release where river stage is maintained at a relatively constant stage

over several months during irrigation season could allow surface water-groundwater connection to occur each year. This gives ample opportunity for observation, monitoring, and characterization of transitions between disconnection to connection and then back to disconnection using repeated ERT surveys.

There are three nearby USGS M2 Group Wells (A, B, and C) 76 m away from the northern bank. Their exact well identification numbers are (24S.2E.19.214a), (24S.2E.19.214b), and (24S.2E.19.214c); their respective well screen intervals are displayed in Figure 4.

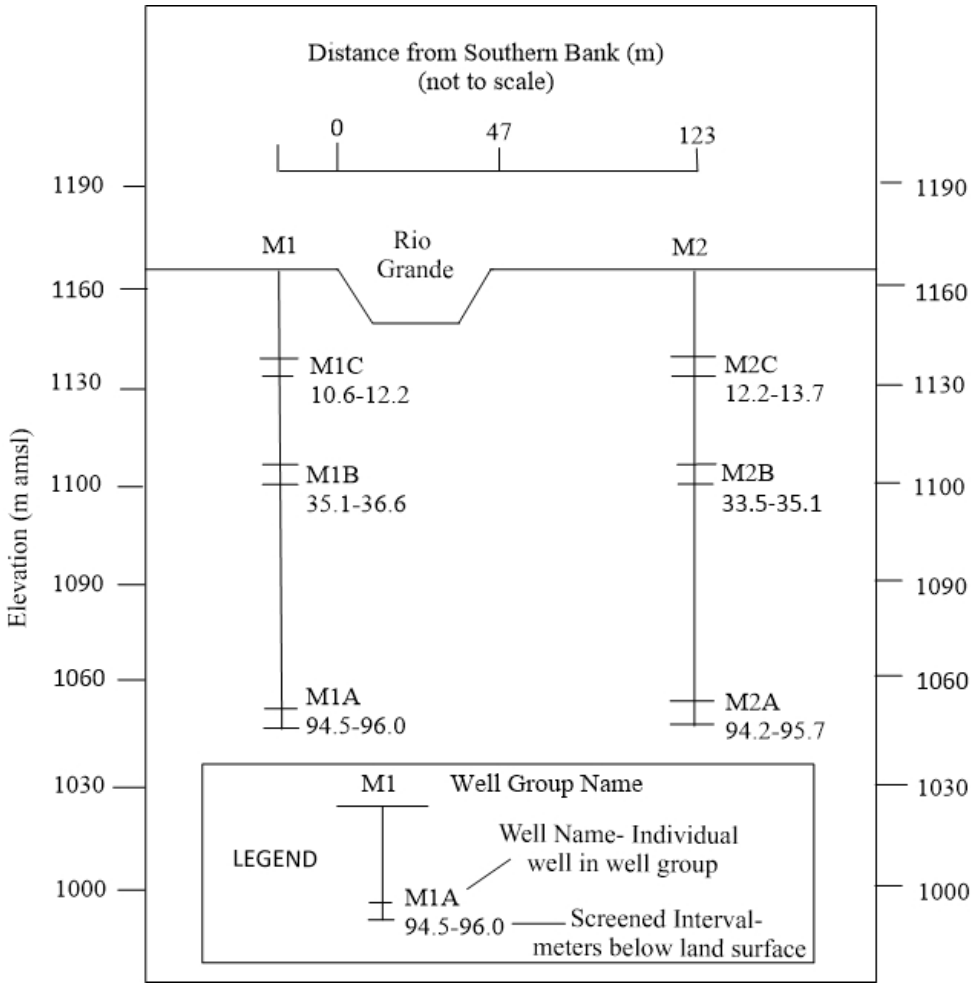

Figure 4. USGS well locations and screen depths alongside the Rio Grande in Mesquite.

The geology of the Mesilla Basin is impacted by the Rio Grande rift; this is a tectonic feature that forms mountains and valleys in which rivers are often confined, thus influencing the path of water flow and therefore the formation of soils composed of unconsolidated alluvial deposits through mechanical weathering. The basin-fill sediments consist of two main geologic units: Rio Grande flood-plain alluvium that consists of clay, silt, sand, and gravel and is generally 18.3 to 24.4 m thick (Nickerson, 1986; USIBWC, 2014), resting above a thicker layer of water-bearing Santa Fe Formation (Teeple, 2017; Ikard et al., 2021; King et al., 1971) that can vary in thickness from less than 30 m to 1127 m (Nickerson, 1986; King et al., 1971). The Rio Grande alluvium is located within the central part of the basin within the incised portion of the Santa Fe Group, and both deposits of alluvium are comprised of clay, silt, sand, and gravel (Nickerson, 1986; USIBWC, 2014). The Mesilla Basin aquifer includes the generally unconsolidated, connected, and continuous alluvial deposits within both formations.

A sediment texture and grain size analysis was carried out by (Humberson, 2021) in 2015 in the shallow subsurface Rio Grande alluvium in the banks of the river at the same location as this investigation (near the ERT transects on Figure 3). The percent composition of three different soil textures in this sample is displayed in Figure 5, displayed from 90%-100% for better resolution of minute amounts of clay and silt grains. This soil is mainly comprised of sandy textured grains (95.7%) with minor amounts of clay (3%) and silt (1.3%) on average for all of the samples (Figure 5). No significant variability in grain size analysis results were observed as a function of depth; no average grain size distribution of a sample was outside of the standard deviation of the average grain size distribution at varying depths, which suggests that the Rio Grande alluvium at the site is relatively homogeneous in grain size and likely hydraulic properties, which is consistent with the available drilling and geologic descriptions from well

installation reports (Nickerson, 1986; USIBWC, 2014). Alluvial and fluvial unconsolidated sediment deposits can be spatially variable (i.e., heterogeneous) in grain size and hydraulic properties. However, significant spatial variability was not observed at this location.

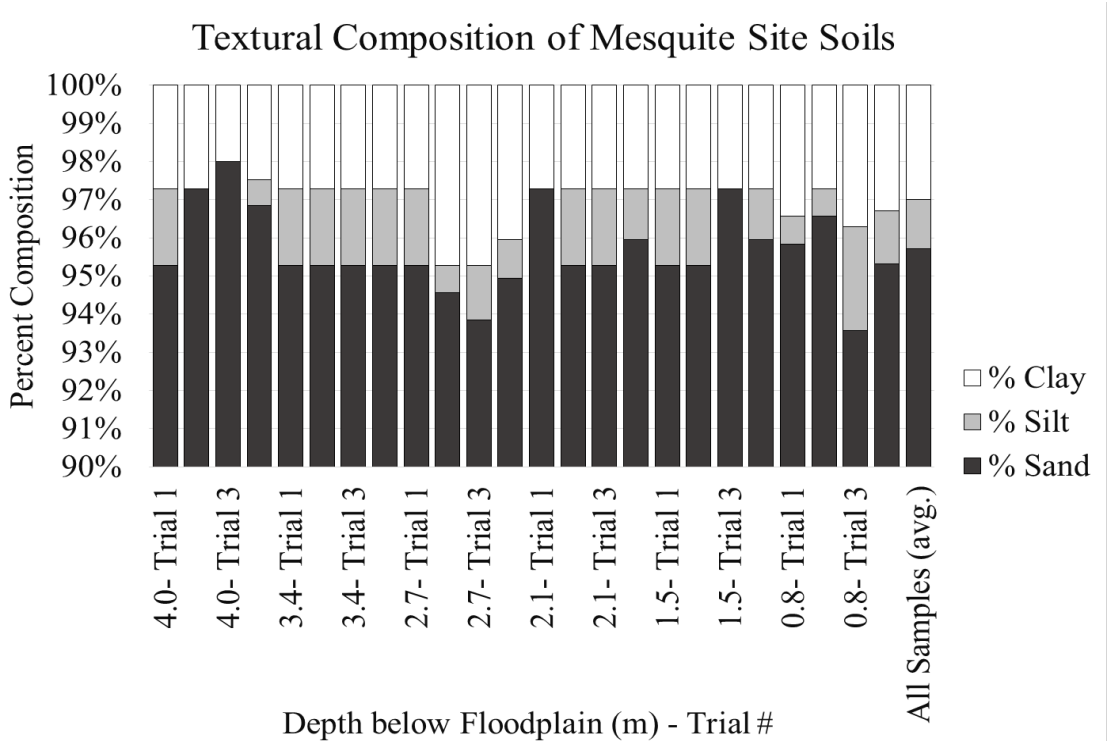

Figure 5. Rio Grande alluvium texture analysis results at the study area site (Humberson, 2021).

The neighboring wells allowed for verification of the location of the water table at the time of resistivity data acquisition. EC of the river water was collected during time lapse ERT measurements to validate the ERT results. The spatial and temporal interpretation of changes in resistivity, supported by groundwater elevation (GWE) and EC data, should be affected mainly by the hydrology of the subsurface geologic formations.

2.2 Electrical Resistivity Mapping

This investigation used time-lapse ERT for mapping the water table below and adjacent to the Rio Grande from March 2020 to December 2020. This method has been validated using

groundwater table monitoring well data obtained from the Elephant Butte Irrigation District (EBID) website (ebid-nm.org) for New Mexico, alongside manual GWE measurements (Figures 3 and 4) within the respective wells and river and groundwater EC data.

ERT measurements were conducted using a SuperSting R8 Electrical Resistivity meter (Advanced Geosciences, Inc., Austin, TX) in the field periodically before, during, and after the presence of water within the Rio Grande. The SuperSting was connected to a patch panel, then programmed to run a 700 mA current through the subsurface for several hours, recording the potential measured from two receiving electrodes. The SuperSting can acquire up to eight simultaneous measurements of voltage during transmission of current on two adjacent electrodes. The ERT measurements were repeated twice during every time lapse ERT data collection event to assess reproducibility and precision. Upon completion, the meter was connected to a laptop, and the data were extracted using the program AGISSAdmin (Advanced Geosciences, Inc., Austin, TX). The dataset was then inverted, and the most probable iterations were generated.

There are multiple types of electrode arrays, or arrangement of electrodes at different intervals, that each present different advantages and disadvantages. The Alt3_Wenner array (Cubbage et al., 2017) was used for this study for its high vertical resolution (Stummer, 2004) for mapping the surface water and groundwater connection, as well as having higher resolution than the unmodified, original Wenner array (Cubbage et al., 2017). The apparent resistivity equation for the Alt3_Wenner array is:

$$\rho_a = K * \frac{V}{I} \quad (1)$$

where ρ_a is apparent resistivity, V = potential difference, I = current, and K = geometric factor (i.e., area divided by length)

ERT using the Wenner Array follows a simple process. The resistivity meter reads information from four electrodes at a time. The four equidistant electrodes are denoted as A, M,

N, and B, which reads left to right in Figure 6. Electrodes A and B are the outermost ones, and are current electrodes, while M and N are the innermost, potential electrodes. Current is discharged into the subsurface through the current electrodes, the electrical potential drop is then determined using the two potential electrodes, and this is considered the direct-current resistivity method. The four-pole Alt3_Wenner array (Cubbage et al., 2017) was used for this investigation, which has the advantage of high resolution, high signal to noise, and significantly more data than the traditional Wenner array, because it adds gradient-type measurements to unused channels in the multi-channel system.

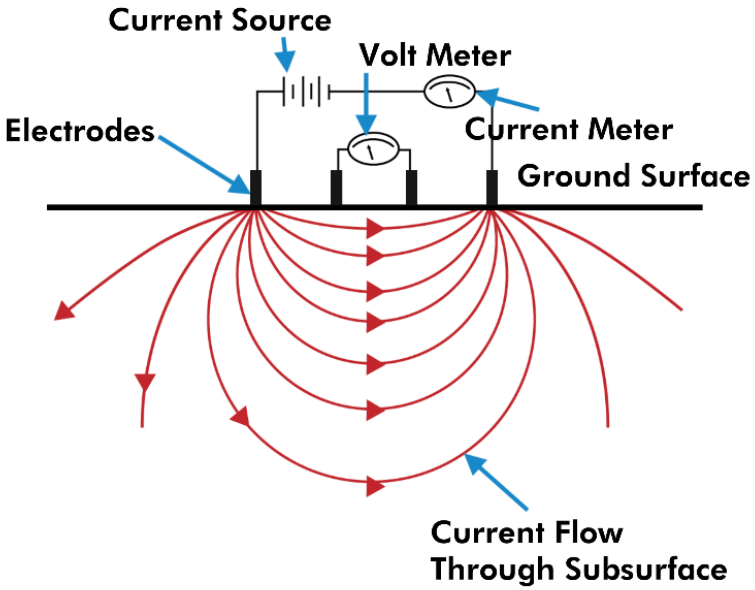

Figure 6. Diagram illustrating electrical current flow through the subsurface using the Wenner Array. Figure from http://edtech.engineering.utoronto.ca/object/electrical-resistivity.

All bulk resistivity data values retrieved from the meter throughout this investigation were converted to conductivity by taking the simple reciprocal for an analogous comparison with the known EC of other waters, and in order to provide an intuitive result for the reader. “Bulk Conductivity” was used to represent these converted values from the ERT geophysical readings.

Induced Polarization (IP) gives a measurement of the chargeability of surrounding materials by measuring the time decay of potential after the current injection is shut off for an ERT measurement. IP is the area under this electrical decay curve (Ntarlagiannis et al., 2016). Variations in IP are associated with heterogeneity in the subsurface due to site pedology and geology, and IP helps with the ERT interpretation, especially finer, clay layers. IP measurements were collected intermittently throughout the irrigation season to be compared to and alongside ERT snapshots.

2.2.1 Inversion

Inversion is an iterative mathematical procedure that calculates the optimized spatial distribution of a physical property (e.g., resistance) measurement combination by minimizing the difference between the measurements and a modeled response. Res2Dinvx64 (Loke et al., 2013) was used for inversion modeling, which incorporated the smoothness-constrained least-squares method (deGroot-Hedlin and Constable, 1990; Sasaki, 1992; Loke at al., 2003). The time-lapse algorithm invoked a temporal roughness filter that minimizes the difference in the resistivity of each model cell and the corresponding cell for the next temporal model (Rucker et al., 2010), guaranteeing that the model was smooth across time and space. It uses this method to estimate the resistivity (and IP) values at numerous, spatially distributed locations in the subsurface and distributed based on the electrode spacing.

2.3 Resistivity Cable Installation

Generally, each dataset had about 3,400 resistance measurements. In order to allow for repeated data collection throughout the irrigation season without any movement or differences in the electrode locations, a cable was installed by burying the insulated, stranded, single conductor, 16-gage copper wire that was clamped to 30 centimeter long “electrodes,” or stainless-steel

stakes, that transmit current into the subsurface at various locations along a cross-section perpendicular to and across the Rio Grande. Data collection configuration at the site included the 56 electrodes at one meter spacing in the channel and shallow banks of the river (photo in Figure 7(a)). Each electrode had contact with the 16-gage copper wire that was connected to a breakout panel (photo in Figure 7(b)). The electrodes and wire were buried within the top 0.5 m of riverbed sediment, and the buried electrodes were not moved after installation. The breakout panel was connected to a multiplexor, which was connected to the SuperSting (photo in Figure 7(c)). An additional 28 electrodes at one meter spacing were added to the northern bank, for a total of 84 electrodes. The other 28 meters of the river transect were set up repeatedly by laying out a cable along the surface of the northern bank for every collection, completing the 84-meter cross-section of interest. Finally, all electrodes and surrounding wells were surveyed using a total station in order to determine the topography of the field site for mapping.

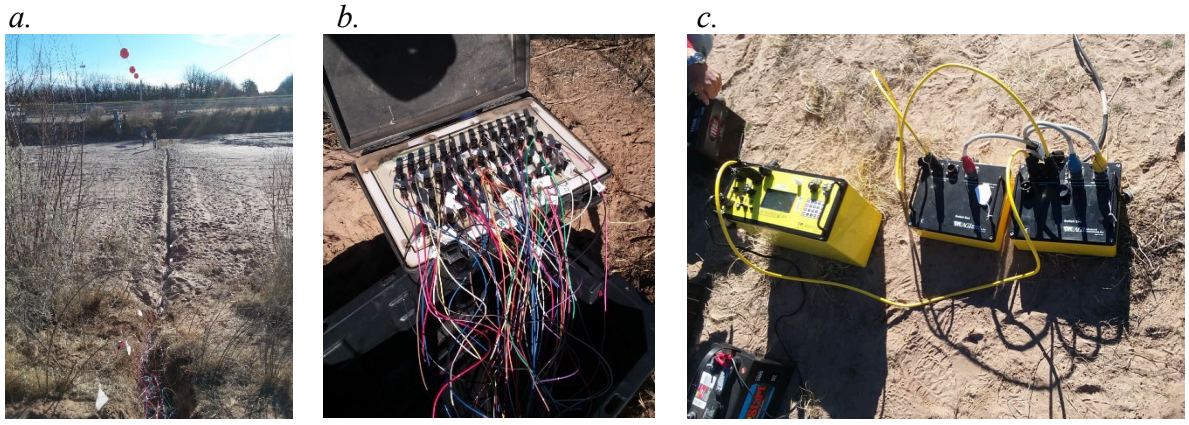

Figure 7. Electrical Resistivity Tomography cable installation within Rio Grande riverbed sediments at the study area in Mesquite, NM, including (a) photograph of transect in which the cable is buried, (b) the patch panel used for conversion from buried cable to the SuperSting, and (c) the SuperSting Resistivity Meter and switchboxes.

2.4 Porosity and Bulk Density of Riverbed Soil

Porosity was calculated using the buoyancy method, assuming the density of the soil particles was 2.65 g/cm^3. This was verified by using the empirical equation:

$$\phi = \frac{V_V}{V_T} \tag{2}$$

where ϕ= porosity, V_V= void volume, and V_T= total volume

The weight of the fully saturated, homogenized soil was recorded, then the soil oven dried at 105°C for 24 hours without burning off the organic matter until no moisture remained. The difference between those values gives the void volume, which was then divided by the total volume to give the porosity. This was repeated four times to calculate the average porosity value, which was needed to use Archie's Law.

2.5 Saturated and Unsaturated Hydraulic Conductivity of Riverbed Soil

The saturated hydraulic conductivity of riverbed soil was determined through two different methods: a) constant head, and b) falling head, and each method was repeated twice. The constant head and falling head methods were performed simultaneously performed. Using a permeameter – which is essentially a cylindrical column with a mesh or a porous stone at the bottom to prevent soil from falling through, and a pipe below the mesh to allow only the eluted water to drain out –water was held at a constant, arbitrary height for an arbitrary amount of time, and the volume of eluted water was recorded. The water was then allowed to drain until the next chosen height was achieved, and the volume was again recorded. This process was used to determine the flow rate, or volume of water over time. With the constant head method, hydraulic conductivity is computed as:

$$K = \frac{V*\Delta L}{A*t*\Delta h} \quad (3)$$

where K = hydraulic conductivity, V = volume, ΔL = change in length, A = area, t= time, and Δh = change in hydraulic head

With the falling head method, hydraulic conductivity is computed as:

$$K = \frac{\Delta L}{t}\ln(\frac{h_o}{h_t}) \quad (4)$$

where h_0 = hydraulic head at time zero, h_t = hydraulic head at time t, and all other units are the same as above

An unsaturated hydraulic conductivity test was completed with the riverbed soil by (Humberson, 2021) in 2015. This consisted of subjecting a saturated soil column to various intensities of negative (i.e., vacuum) pressure and measuring the volume of water that eluted. More on this method can be found elsewhere (e.g., Shukla, 2013). From the unsaturated pressure and water content values, a Retention Curve (RETC) model determined the van Genuchten parameters (i.e., n, alpha, and residual and saturated water content) by utilizing nonlinear least-squares analysis to optimize parameters by minimizing differences between the model and observations (van Genuchten et al., 1991). The soil samples from 2015 and 2020 had nearly identical hydraulic conductivity and bulk density values, supporting the use of previous data and its relevance.

2.6 Pore Water Conductivity vs. Bulk Conductivity

Laboratory experiments were developed to determine the mathematical relationship between pore water EC and bulk electrical conductivity (which includes EC of the water and also the solid minerals). The experiments were carried out using a bench top scale soil-water system, consisting of a plastic box filled with soil with four electrodes inlets as illustrated in Figure 8.

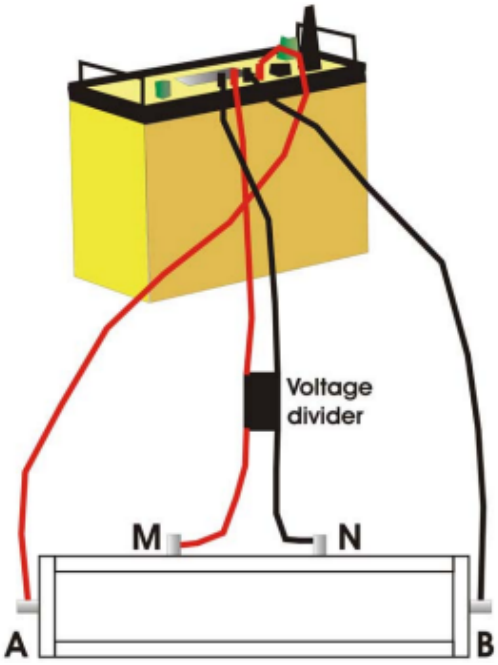

Figure 8. Diagram illustrating the bench-top scale laboratory electrical resistivity measurement method (Advanced Geosciences, Inc., Austin, TX).

The assembly shown in Figure 8 is essentially a small-scale replica of a larger resistivity measurement that would be collected at a field site. The resistivity is given as

$$\rho = \frac{R*A}{L} \tag{5}$$

where ρ=Resistivity, R=Resistance, A=Cross-sectional Area, and L=Length of the Box

One soil sample was used for each trial, and water saturation was increased by increments of volumetric water content until the soil reached saturation. The resistivity measurement at each water saturation value was repeated three times. When water was added, the soil was transferred into another container, mixed with the water, then put back into the box, taking care to not let extensive evaporation or change in temperature occur. The max current was set to 1 mA, with a measurement time of 1.2 s and max error of 2%.

2.6.1 Regression Model for Saturation Relationship

The relationship between water saturation and bulk resistivity was developed using the data from the pore water conductivity vs. bulk conductivity testing, and applying it within a derivation from Archie's Law:

$$\log\left(\frac{\rho_b}{\rho_w}\right) = \log(a) - n\log(S) - m\log(\phi) \quad (6)$$

where ρ_b is bulk resistivity, ρ_w is water resistivity, S is saturation, ϕ is porosity, and a, m, and n are fitting parameters

A simple linear regression was used to solve for the fitting parameters a, m, and n. This was useful for converting site conductivity to saturation and vice versa.

RESULTS AND DISCUSSION

3.1 Geophysical Results

Figure 9 displays 2D conductivity snapshots from March 11 to December 4, 2020. The Rio Grande water arrived at the site location on March 15, and started draining from the site location on September 29. Water was yet to arrive at the monitoring site on March 11, so this date established a background (dry) conductivity. With the arrival of river water, the shallow subsurface below the riverbed became more conductive than on March 11 due to an increase in water saturation from infiltration. Water is more conductive than air, and so the bulk resistivity decreases and bulk conductivity increases with a transition to water saturated conditions. After river water was drained and no longer present on December 4, the site conductivity returned to the background conditions observed on March 11, this time associated with a decrease in water saturation and a transition back to air-filled pore spaces. Regarding the middle three snapshots (March 15, 16, and 17), there is little change in conductivity, until the site is dry again on December 4, as quantitatively confirmed in Figure 10. The left-hand side of the plots 0-20 m from the northern bank show high conductivities (2.6-2.8 μS/cm) due to the presence of a steel well casing at that location, and not pore water. Overall, the conductivity captured using ERT increased when water was present in the river and infiltrating into the groundwater, and conductivity decreased when water was no longer present in the river and was draining from the groundwater into the shallow subsurface. The GWE of M2C also rises and falls with the river water elevation and presence of water, validating the use of ERT for water table mapping.

The wet-up period where partial river-groundwater connectivity interactions would have been observed was missed. The transient wet-up and connection between river and groundwater occurred within or less than within one day, but the ERT monitoring was not conducted with a

high enough temporal frequency that would have allowed for measurement of these transient changes. This suggests rapid mixing and cycling within the hyporheic zone, establishing full connectivity within as little as 24 hours of water reaching this site. For the 2020 irrigation season, the transition from dry background conditions (disconnected) to the arrival of water (connected) and back, however, was captured using ERT. In general, the transient changes in ERT response at the river flooding arrival (decreased resistivity and increased bulk EC with increased riverbed water saturation) and at river flooding recession (increased resistivity and decreased bulk EC with decreased riverbed water saturation) are attributed to the transition to connection and then transition back to disconnection, respectively. For this particular location, these transitions occur rapidly, although the transition occurs more slowly for the river flooding recession. These results confirm that time-lapse ERT can be used to monitor and assess the connectivity transitions for ephemeral or intermittent streams and rivers. However, subsurface resistance is not a direct measure of water saturation, and other impacts on this geophysical measurement response should also be considered.

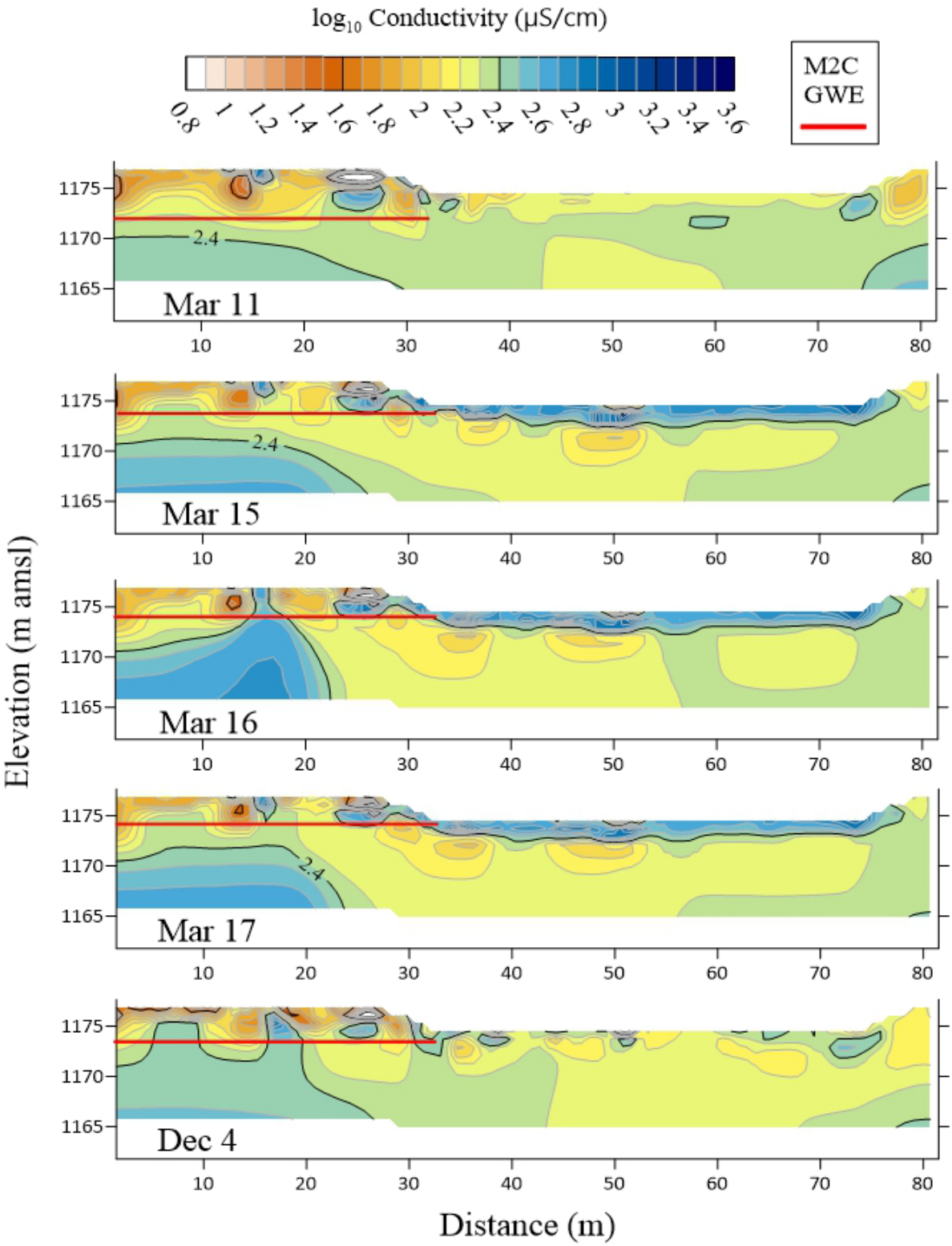

Figure 9. Contour plots of ERT measurements in bulk conductivity conducted at different days in March and December; the red line indicates the elevation of the groundwater table (GWE) measured at the adjacent groundwater well.

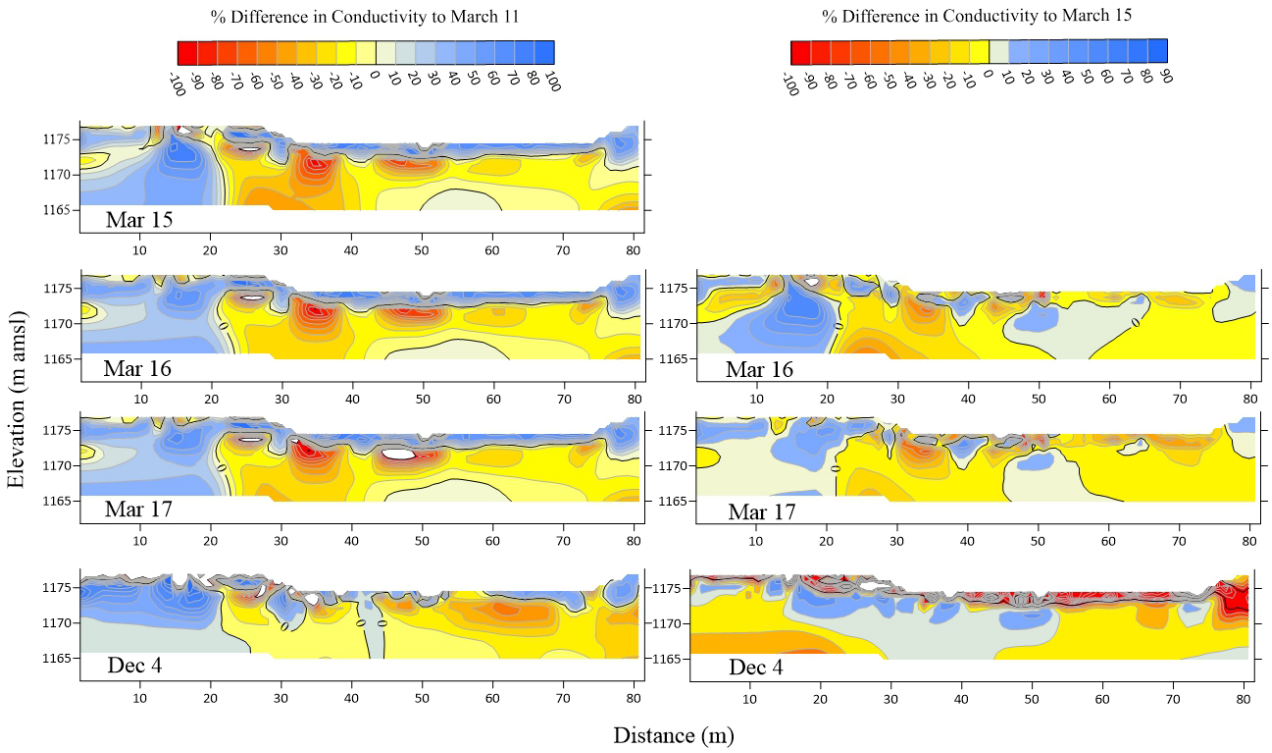

Figure 10. Contour plots of the percent differences in ERT bulk conductivity for several snapshot measurements compared to conditions when the river was absent (March 11) and present (March 15).

The left-hand side of Figure 10 displays daily snapshots with a comparison in percent difference in conductivity to when water in the river was absent on March 11. Since water in the river was present from March 15 to 17, these plots show large (50-100%) differences in conductivity indicated with the blue shades compared to March 11 in the shallow subsurface, associated with the water infiltration and thus increase in water saturation. The right-hand side of Figure 10 compares each snapshot to March 15, when water in the river was present, so for March 16 to 17 where water was still present, there was minimal (from -10 to 10%) difference in conductivity indicated with the yellow-orange shades, because those three representative wet snapshots are nearly identical to one another. Not having a significant change between these wet snapshots further supports that ERT changes were primarily caused by changes in pore water

saturation. It should be noted that the shallow subsurface had a different and nearly inverse conductive response to the underlying, deeper region of the subsurface.

When displayed side-by-side with the conductivity snapshots on the same day, one can see that the IP (chargeability) does not vary with or without the presence of water; the riverbed remains a bluish color that signifies a low (1 to 8 mV/V) chargeability, even while changes in bulk conductivity were observed. Because IP data can differentiate pedology and geology, these uniform and unchanging IP results on the right-hand side indicate no significant amount or layering of clay, and that the site is relatively homogeneous, which matches the available well report geologic descriptions. It appears that the riverbed composition and sediments underlying the riverbed including shallow alluvium at this study site are geologically homogeneous (Figure 11), yet the hydraulics vary with depth (Figures 9 and 10).

It is not known exactly how the Rio Grande alluvium and Santa Fe Formation soils are separated and where the contact point is at this study site. The shallow, sandy sediments that comprise the Rio Grande alluvium appeared to become saturated and also drain water quickly. The deeper sediments became more conductive than the shallower sediments, and the water table began to drop. Based on rapid changes in both the near surface and deeper materials, it is clear there is a strong hydraulic connection, despite the direction of bulk EC changes through time. A gradient self-potential logging was completed by Ikard et. al. (2021) along the Rio Grande including this study site; Ikard et al. concluded that two different aquifers exist in this area, which was indicated by variations in saline groundwater seepage through both soil profiles into the Rio Grande, and this supports our findings. Ikard et al. (2021) also noted the hydraulic connections between upper and lower formations with a floating self-potential array conducted in July 2020. Near the study site (1.9 km up-gradient) and just below the Mesilla Dam, they noted a

change in condition from a net losing condition upstream to a relative mild gaining condition immediately downstream, as groundwater was conveyed beneath the Mesilla Dam and back into the channel downstream. These observations may partly explain the distinct bulk EC patterns in the near surface versus deeper sands.

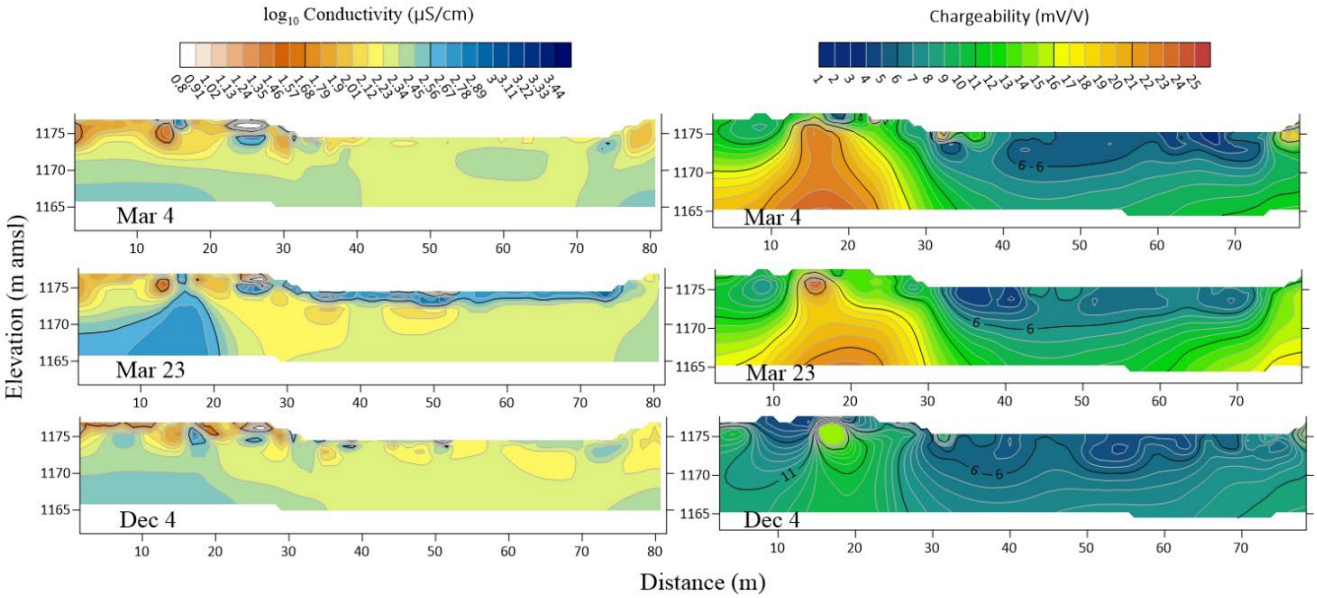

Figure 11. Contour plots of data collected on March 4, March 23, and Dec. 4 for comparison of ERT bulk conductivity (left panel) to induced polarization (right panel) results.

3.2 Flow, Electrical Conductivity, Temperature, and Elevations of Site Waters

Figure 12 depicts the elevations of both the river and groundwater, as well as the river flow rate throughout the irrigation season before, during, and after water was present. The increase in flowrate and elevation is associated with the release of water from the Elephant Butte, Caballo, and Mesilla Dams in March, and contrarily there is a large decrease when water was shut off to the site in September. The GWE of wells M1C and M2C respond similarly to the river elevation, following minor pervasions in river flow and even displaying a similar response to the river with the arrival of water on March 15, 2020. For example, the GWEs of the shallow wells

increase simultaneously with river infiltration, which indicates that they are hydraulically connected and void of a separating layer (or clogging layer) between them. The shallow wells are part of the same Rio Grande alluvium aquifer that interacts with the river. The river drained after the Dam release cessation, and the system transitioned back to a disconnected river and groundwater system, which illustrates the reversibility of the disconnection process. This reversibility of the disconnection process is consistent with a prior publication that focused on drought in an upstream sub-basin (Fuchs et al., 2019).

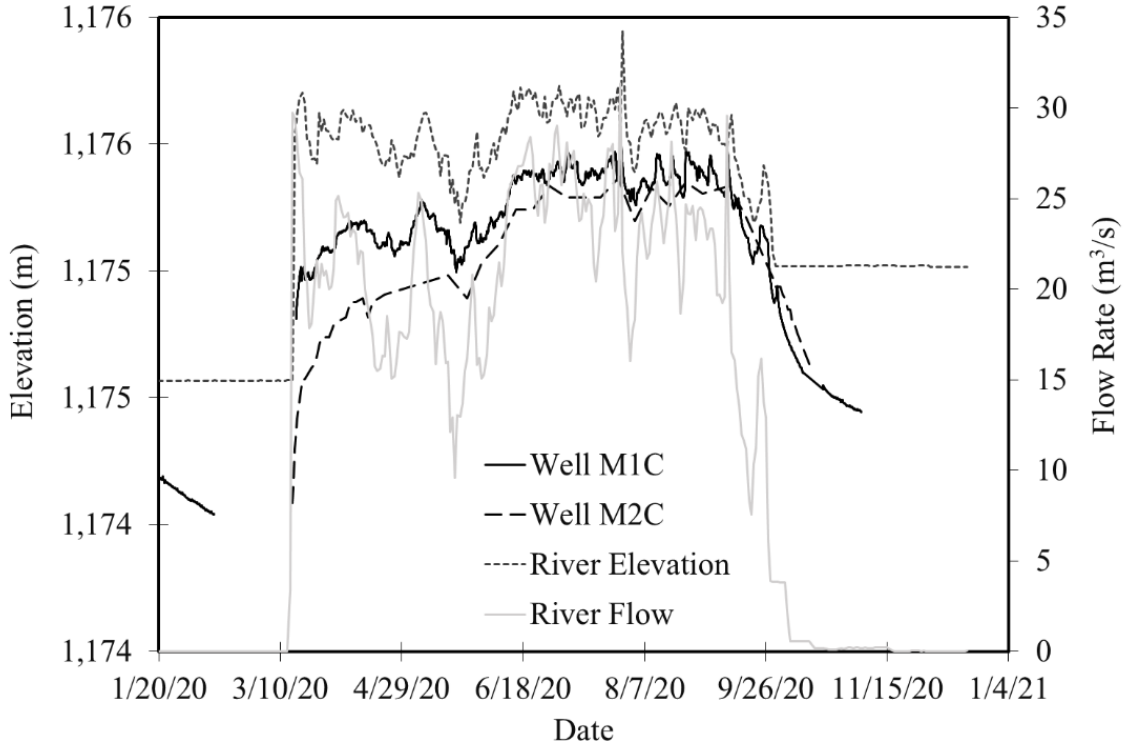

Figure 12. Comparison of transient river flow rate, river elevation, and groundwater elevation before, during, and after the irrigation season.

As observed in Figures 9 and 10, the shallow subsurface had a different and nearly inverse conductive response compared to the underlying, deeper region of the subsurface. Due to this, for further comparisons between bulk conductivity and other variables, one representative "shallow" location (x= 55.5 m, z= 1173 m) and one representative "deep" location (x= 55.5 m,

z= 1171 m) were chosen. The transient bulk conductivities of these points are displayed in Figure 13, amongst other variables. The shallow bulk conductivity varies similarly to the river flow rate, while the deep bulk conductivity remains relatively constant throughout the irrigation season. The apparent relationship between shallow bulk conductivity and river flow rate supports the assertion of rapid infiltration within the hyporheic zone at this site, as well as hydraulic connectivity between the river and shallow groundwater captured with ERT.

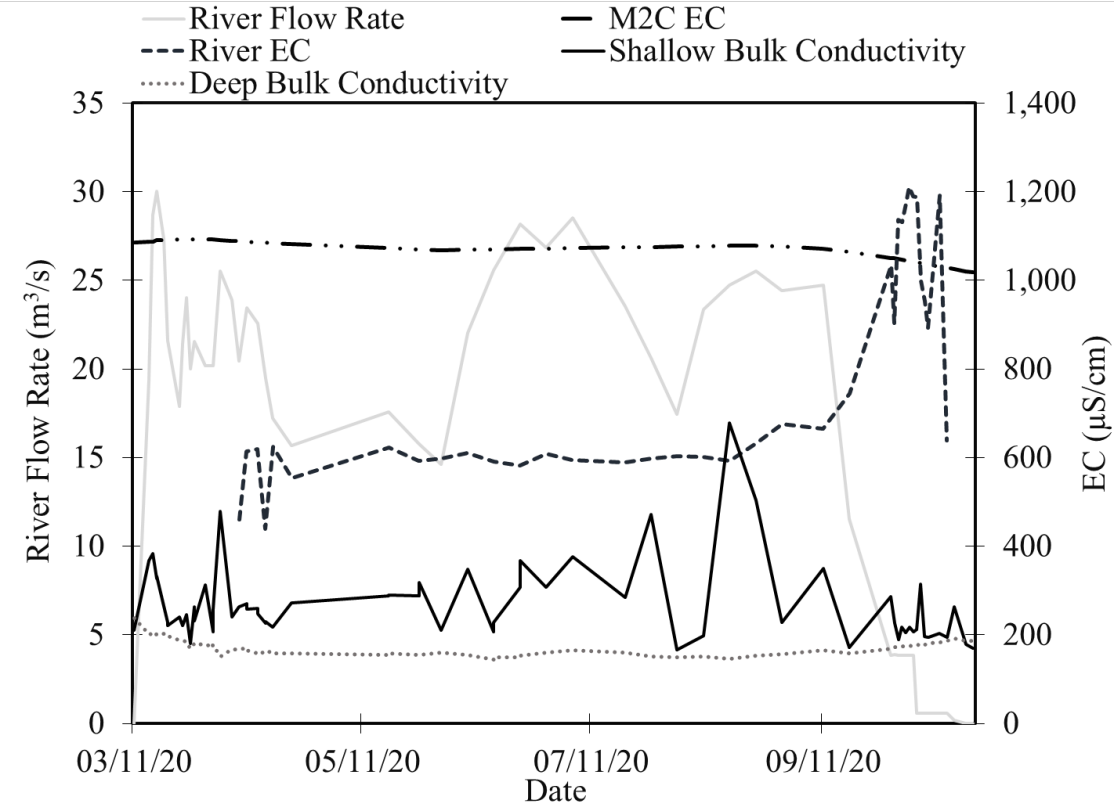

Figure 13. Comparison of transient shallow and deep ERT bulk conductivity, river flow rate and EC, and groundwater EC at well M2C.

There is a spike in the river EC after mid-September when the water drained following the halted release from upstream dams, but well M2C EC remained relatively constant (Figure 13). The river EC increased from ~600 µS/cm to that of a similar EC of well M2C, which was an almost constant ~1,000 µS/cm. The EC of source water from Caballo Dam was a relatively

steady ~600 µS/cm throughout 2020 as well (ebid-nm.org). This suggests that while the dam is releasing water from the upstream reservoir, the reservoir water is the source of water discharge at the Mesquite site (since the water EC values match). Then, when the dam was closed around mid-September, the flow declined with removal of that source of water, and the EC of the remaining river water increased to match the EC of the groundwater, which suggests that the source of water to the river at this Mesquite site changed with EC from the upstream reservoir to the groundwater. This is caused by saline groundwater seepage into the Rio Grande only in the later time of the irrigation season, and not earlier in the season when there was a larger amount of river water supplied from the upstream reservoir dam releases. The system was a losing stream during the early and middle time of the irrigation season, and then it briefly transitioned to a weak gaining stream system at the end of the season when the dam discharge ended. The river water equilibrated, in terms of water EC, with the groundwater at the shallow well late in the irrigation season, but the shallow groundwater EC was relatively constant due to infiltration in the early part of the season. It is possible that the groundwater well was not positioned to monitor groundwater EC changes due to river infiltration, and the groundwater reservoir may have been large enough that minor infiltration of low EC river water did not cause significant changes in groundwater EC. The laboratory experiments conducted to determine the relationship between pore water conductivity (i.e., river EC) and overall bulk conductivity (see Appendix, Figure 20) showed that these variables are positively correlated, with an R^2 value of ~0.96, which is generally supported by Figure 13 with the shallow bulk conductivity curve.

In Figure 14, the GWE of shallow well M2C varies with and responds to the river elevation. Contrarily, the GWE of the deeper wells, M2A and M2B, do not. Based on the well screen installation depths also shown in Figure 14, it is reasonable to conclude that the well

screen of M2C is within the Rio Grande alluvium aquifer and the deeper well screens are within the underlying Santa Fe Formation, which appear to be hydraulically different from each other (Teeple, 2017); yet there is no evidence of a confining layer existing between them. The larger fluctuations in deeper wells M2A and M2B are associated with groundwater well pumping from the deeper Santa Fe Formation aquifer. If all three of the M2 group wells were hydraulically connected to the same aquifer, one would expect them to have a similar hydrologic response. However, the lack of GWE fluctuations in the shallow well M2C suggests that the deeper system including wells M2A and M2B appears to be hydraulically disconnected from both M2C and the river system, at least during this one-year study period, before a lag infiltration into the deeper Santa Fe Formation has had time to occur and be observed. The distance between well M2C and the deeper well pumping, and also the amount of river recharge, are also likely to have caused the attenuated impact of pumping within the shallow groundwater near M2C.

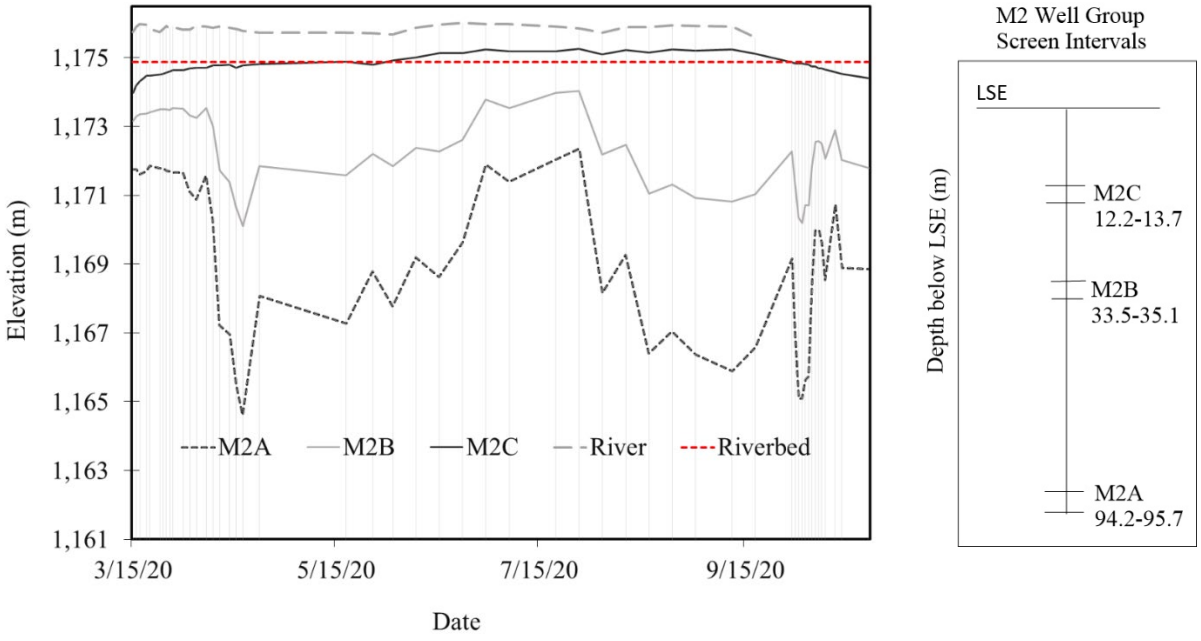

Figure 14. Comparison of transient water elevations of the Rio Grande and groundwater elevations in adjacent wells, alongside the screen interval for each well. Each vertical line corresponds to a date of ERT data collection.

According to Figures 13 and 14, the behavior of ancillary data such as EC and GWE showed changing responses throughout the irrigation season. In order to investigate these temporal changes, the irrigation season was divided into two parts: "early" and "late" irrigation season. "Early" indicates the time period from March 15 to September 11, 2020 (i.e., when upstream dams were releasing significant amounts of water), and "late" is from September 18 to October 14, 2020 (i.e., when upstream dams were not releasing much water). Thus, the whole irrigation season is from March 15 to October 14, 2020. Table 1 quantifies the correlation coefficient between river elevation and each listed variable.

Table 1: Correlation coefficients of M2A, M2B, and M2C GWE with river elevation.

Part of Irrigation Season	M2A GWE	M2B GWE	M2C GWE
Whole	0.312	0.363	0.142
Early	0.256	0.259	0.173
Late	-0.191	-0.193	0.697

A correlation coefficient is a number between -1 and 1 that indicates the relationship or lack thereof between two variables. Negative numbers signify a negative (i.e., inverse) relationship, and positive numbers signify a positive (i.e., direct) relationship. The closer the numbers are to -1 or 1, the stronger the correlation. Denoted in red in Table 1, the number 0.697 is a good correlation. This means that M2C GWE and river elevation are well correlated during the late irrigation season. This is reasonable because we know that M2C GWE has a similar response to the river elevation, and they both decrease when the water is shut off from flowing to the Mesquite site. However, in Figure 14, M2C GWE and the river elevation visually appear correlated throughout the whole irrigation season, and not just the late season as indicated with

the correlation coefficient; this is due to other dynamics transpiring in the groundwater that is not observable in the river, such as flood irrigation. There are no other notable correlation coefficients for M2A and M2B GWE; in particular they are not correlated with river elevation, which is in agreement with the claim that deeper wells M2A and M2B are in a hydraulically distinct aquifer system from the river, at least during this investigative timeframe of one year.

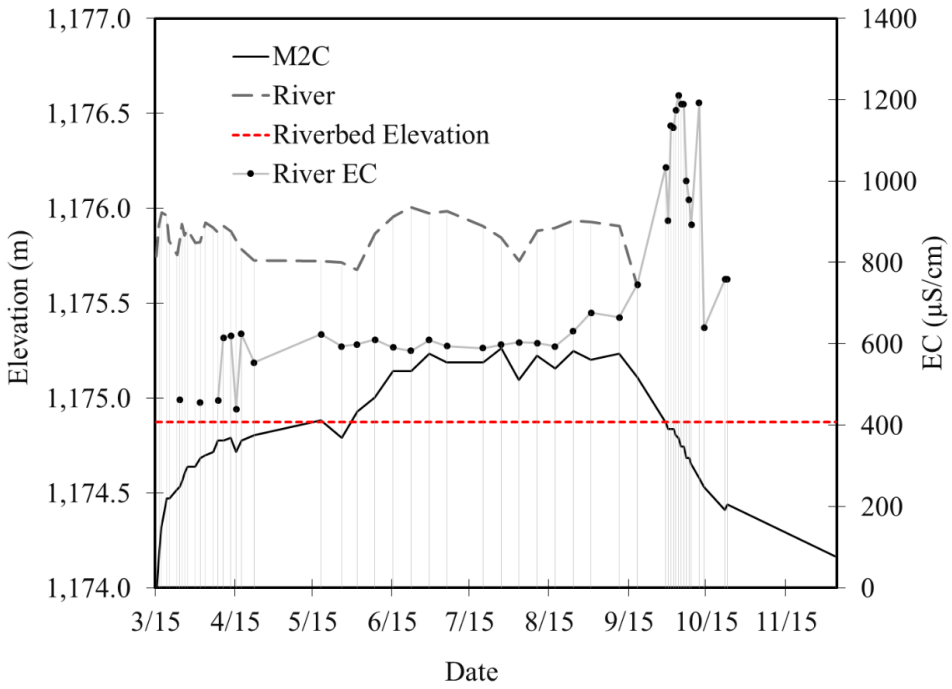

Figure 15. Comparison of transient water elevations and EC of the Rio Grande and groundwater elevations at the M2C well, alongside the screen interval for each well. Each vertical line corresponds to a date of ERT data collection.

Figure 15 is similar to Figure 14, but without the GWEs of M2A and M2B, and River EC was added for higher resolution and focus on the shallow system fluid flow and saline solute transport. For most of the year, the system is losing water while the river water elevation (i.e., stage) is greater than the GWE in M2C, and thus the hydraulic gradient is in the direction of flow from the river to the groundwater. However, a reversal to an upward hydraulic gradient (i.e., groundwater flow to river) has been observed in the southern Mesilla Valley (Teeple, 2017), and

there is a mild predilection for this behavior downstream from the Mesilla Dam at our investigation site (Ikard et al., 2021). Therefore, there may have been a period later in the irrigation season between mid-September and mid-October where a transition to a gaining stream occurs when the river elevation is below M2C GWE (or GWE adjacent to the river banks), which is reinforced by the findings from Figure 13. This does coincide with the temporary spike in river EC when the river EC then matches the EC of the adjacent groundwater monitoring well, which is evidence of groundwater upwelling into the Rio Grande only during the short time period after the dam reservoir water is shut off. This late-season groundwater discharging to the river may have been, in part, derived from water that was infiltrated from the river to the groundwater earlier in the season, which is termed return flow.

The transient bulk conductivities for the previously selected shallow and deep point of the subsurface are shown in Figure 16. The shallow bulk conductivity point has greater variability throughout the investigation period compared to is the deep bulk conductivity point. This response is mainly associated with changes in water saturation (Figure 9). The deeper zones stayed completely water saturated throughout the year, and ERT bulk conductivity for the deeper zones varied over time only due to changes in salinity and temperature. However, the shallow zone was unsaturated with respect to water filling pore spaces when the river was not present, and the shallow zone pores became completely saturated as the groundwater connected with the river while the river was present. The high conductivity of water caused increased changes in ERT bulk conductivity when the surface water and groundwater became connected since there was more water present and filling the pores. According to Teeple (2017), the hydraulic conductivity is much greater in the shallow subsurface with values as high as 22 meters per day (m/d), and it only decreases with depth. This highly permeable shallow subsurface influences

rapid seepage/infiltration, explaining in part the greater ERT dynamics in the shallow subsurface as well as why the initial ERT snapshot time interval of days/weeks failed to capture the stages between the transition from fully disconnected to fully connected.

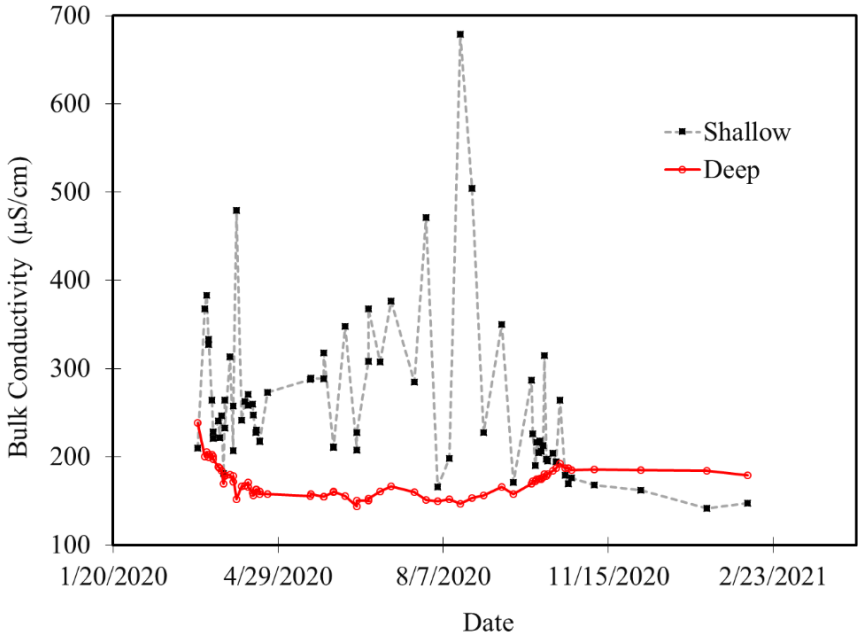

Figure 16. Transient results of ERT bulk conductivity comparing data from a shallow location and a deep location in the subsurface.

When observing the shallow bulk conductivities versus the water conductivities within the shallow well and the river in Figure 17a, it is evident that the water conductivities from both river and groundwater are relatively different from each other until the late irrigation season when the river EC spike was recorded. Also, the shallow bulk conductivities have a large range from ~200 µS/cm to as much as 700 µS/cm throughout the irrigation season. This significant range of variability is not observed in the deep point shown in Figure 17b, which primarily ranges from 150 µS/cm to 200 µS/cm. This suggests that the bulk conductivity is more variable due to saturation in the shallow subsurface than the deep zone, which is not as affected because it is already saturated.

Regarding the deep bulk conductivity, the river and groundwater conductivities have significantly more overlap or similar values. The deeper, Santa Fe Formation, system is likely more influenced by additional infiltration from upstream because of more pumping in deeper wells that augments the hydraulic gradient and the groundwater flow direction. At the study site, the groundwater elevation is closer to the river stage than it is upstream, thus giving very little hydraulic gradient to drive either infiltration and river seepage or return flow (even though there is evidence that both occur at this location).

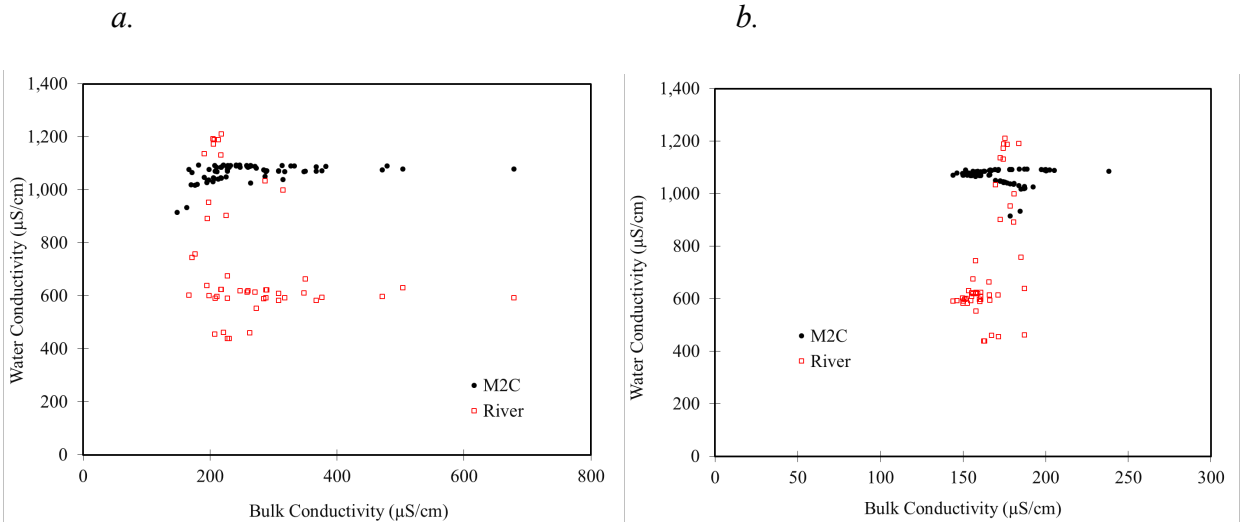

Figure 17. Comparison of shallow (a) and deep (b) ERT bulk conductivity plotted as a function of river water and groundwater electrical conductivity.

3.3 Correlation Coefficient Analysis

The correlation coefficient plots in Figure 18 provide visual confirmation and a summary of the findings within the previous charts and graphs. One can see spatially dynamic relationships between each variable with bulk conductivity at every point in the entire measurement profile. The individual correlation coefficient value of both selected representative shallow and deep points for each profile during the listed dates is directly labeled in bold and

italics on each contour plot, which is relatively close to the exact locations as well (as stated previously, the shallow point is x= 55.5 m, z= 1173 m and the deep point is x= 55.5 m, z= 1171 m). The time frames for each one differ because they were constrained to when data for each variable could be measured, but are covering the whole irrigation season as much as possible.

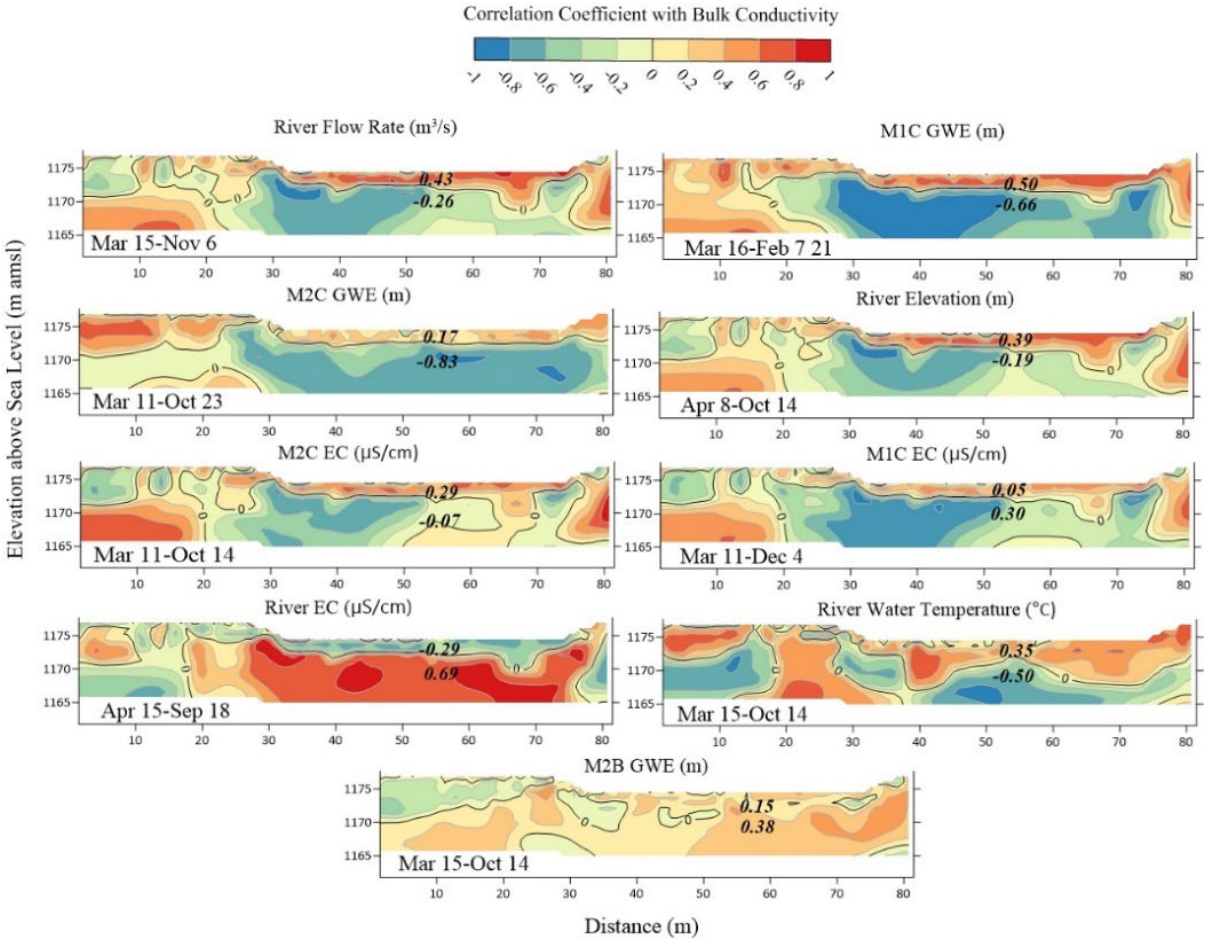

Figure 18. Contour plots of correlation coefficient results of various variables with ERT bulk conductivity, and the spatially averaged correlation coefficients for the shallow and deeper regions are in bold and italics. Results are plotted with measurement dates labeled that were used in the correlation analysis.

The top six contour plots in Figure 18 are visually similar in that there is a thin layer of red at the top meaning a positive correlation, and blue meaning a negative correlation at deeper zones. In other words, for each variable in the top six plots (river flow rate, M1C GWE and EC,

M2C GWE and EC, and river elevation), the shallow subsurface is directly correlated with bulk conductivity, while at lower depths the variable is inversely related to bulk conductivity. River flow rate is directly correlated with bulk conductivity in shallow depths because water infiltrates quickly into the shallow subsurface, and it is empirically known that the more water-saturated soils are, the more conductive they will be. The next three plots: M1C and M2C GWE, and river elevation, show a similar response for the same reason. GWE increases with river elevation since the surface water and groundwater are connected, and the presence of the river causes GWE increases or mounding. Both of these cause pore water saturation, and this increases the bulk conductivity. Therefore, these four results are driven by changes in water saturation, and are supported by Figures 11, 13, and 17. M2C and M1C EC are the last two plots on Figure 18 that display a positive correlation in the shallow subsurface and an inverse correlation at deeper points. It makes sense that as shallow well water becomes more conductive, then the bulk conductivity would follow suit. However, the opposite of this relationship with depth can be explained by agricultural pumping of deeper wells and deeper aquifer conductivities mostly influenced from upstream river infiltration and also lateral flow and pumping, which is supported by Figures 16 and 17.

The exact opposite is seen in the River EC contour plot of Figure 18. As river EC increases, the shallow bulk conductivity decreases, which is not what one would expect without the context of the study area. It should be noted that the last date for this contour plot was September 18, before the water started draining. This is because during the early irrigation season, the main determinant of the river EC is the EC of the water from upstream, which is substantially lower than the EC of the groundwater (see Figure 13). Because the river water is

less saline than the groundwater during this time, the bulk conductivity decreased in the shallow subsurface due to river water infiltration into the shallow subsurface.

The river water temperature plot included in Figure 18 shows that most of the contours are orange/red, meaning temperature is positively correlated with bulk conductivity, in agreement with the definition of temperature and conductivity (i.e., the faster molecules vibrate the higher the temperature, the faster a current can jump between them/be more conductive). It also suggests that temperature is a variable affecting the bulk conductivity, but not as strongly as fluctuations in water saturation. Lastly, the M2B GWE plot shows correlation coefficients between -0.2 and 0.2, so there is essentially no relationship between M2B GWE and bulk conductivity, as expected. M2B is one of the deeper wells that seems to be hydraulically separate from the river and shallow groundwater system during this study period (but there is no evidence of a confining layer existing between the Rio Grande alluvium and Santa Fe Formation), supported by Figure 14 and Table 1.

One final display of the relationships between the gathered ancillary data and the bulk conductivity from the geophysical snapshots is represented in Table 2. It is similar to Figure 18, but separates different parts of the irrigation season, and is a numerical table for the correlation coefficient for the variables and times specified for the representative “shallow” and “deep” points selected earlier. The numbers indicated in red signify a considerably high correlation. The coefficient between river flow and bulk conductivity at the deeper point and during the late irrigation season is -0.898, and thus inversely correlated. This could be observed only in the late season because of a lag in infiltration and transport, which likely was due to the increased infiltration that occurred upstream as noted by Ikard (2021). M2C and M1C GWE are inversely

correlated with deep bulk conductivity throughout the whole irrigation season and when divided into separate parts, with respective coefficients of -0.828 and -0.660.

Table 2. Correlation coefficients of river flow, river and groundwater EC, GWE, and temperature with ERT bulk conductivities; results are presented for the shallow and deeper regions with correlation conducted over the early, late, and entire time of monitoring during the irrigation season.

Depth	Part of Irrigation Season	Flow	River EC	M2C EC	M2C GWE	M1C EC	M1C GWE	Temperature
Shallow	Whole	0.427	-0.294	0.290	0.175	0.046	0.502	0.353
	Early	0.372	0.117	-0.164	0.198	-0.297	0.282	n/a
	Late	-0.166	0.149	0.188	-0.083	0.607	0.481	n/a
Deep	Whole	-0.256	0.690	-0.066	-0.828	0.301	-0.660	-0.501
	Early	0.216	-0.080	0.618	-0.836	0.602	-0.783	n/a
	Late	-0.898	0.036	-0.945	-0.988	-0.337	-0.681	n/a

CONCLUSIONS

A river-groundwater intermittent connectivity monitoring approach using a time-lapse ERT monitoring was developed and implemented for one year along an intermittent, ephemeral portion of the lower Rio Grande in southern New Mexico, to investigate temporal and spatial river-groundwater connectivity variability. Subsurface electrical resistivity, river-groundwater EC, and river-groundwater elevation data were collected periodically in the Mesilla Basin along a cross-section of the lower Rio Grande downstream from the Mesilla Dam near Mesquite, NM during the 2020 irrigation season. The resistivity data were collected along 84 meters of the riverbed and up onto both banks. A cross-section transect perpendicular to the channel length was used for ERT monitoring along with ancillary hydrologic data, including river-groundwater EC, river-groundwater elevation, and surface water temperature collected periodically at the lower Rio Grande. All data were acquired during the 2020 flood release from the Elephant Butte reservoir between March and December 2020. Resistivity correlation analyses were then developed with the ancillary data to elucidate the primary drivers behind the resistivity changes, ultimately leading to a greater understanding of connectivity along this very important riparian system.

Time-lapse ERT changes were used to characterize the transient and spatial connectivity transitions. Temporally, the electrical resistivity geophysics showed that, at the onset of river flow and throughout the active flooding season, the shallow materials became very conductive in the top two meters. The change to conductive sediments was attributed to the transition from disconnection to connection and saturation of the pore space with river water that warmed throughout the season. Results have shown resistivity changes primarily due to variations in water saturation and with some influence from temperature and aqueous EC (i.e., salinity)

differences between resident groundwater and the infiltrating surface water. Below this layer, the conductivity of deeper sediments changed to a lesser degree and out of phase with the upper sediments. ERT changes were able to characterize the transition from disconnection to connection and back to disconnection, since the ERT response during that short time period was primarily attributed to changes in water saturation. During the majority of the monitoring, and when the river-groundwater system was connected, we hypothesized that the most likely dominant control of the observations of connectivity was through the changes in surface water temperature, which acted as a tracer for resistivity. Throughout the flooding season, the river water warmed until late August. During the same period, the bulk EC in the shallow sediments increased. After August, both datasets showed declining values. An inverse relation was observed for the deeper sediments within the groundwater. We explained these observations by noting the direct impact of warming surface water on shallow bulk EC. For the deeper groundwater, the results likely show a lag in arrival of the temperature signature of upwards to 180 days, but further evidence is needed. Our hypothesis fits within the framework of research by Ikard et al. (2021) which mapped losing and gaining reaches along the lower Rio Grande. At the Mesilla Dam, the stream was considered losing in July 2020, and transitioned to gaining closer to Mesquite. Further, influences of warming groundwater at the top of the water table within the conductivity analyses were observed, providing evidence of mixing surface water with groundwater and the temporal nature of observing their connectivity through temperature. After connection occurred while water saturation was constant, time-lapse ERT changes were likely dominated by temperature, which allows for infiltration monitoring using heat as a tracer.

The results also varied spatially due to the presence and location of two hydraulically distinct aquifers: shallow Rio Grande alluvium aquifer and deeper Santa Fe Formation aquifer.

The observed late-season spike in river EC to values similar to the conductivities observed in shallow groundwater affirm the hypothesis that transitory conditions from losing stream to mildly gaining stream conditions during the late irrigation season occurred. This is supported by previous investigations where it was demonstrated that the study location has a propensity to transition to a gaining area due to differences in elevation, temperature, and conductivity between resident groundwater and surface water (Ikard, 2021). We recommend that electrical resistivity geophysics be incorporated in long-term studies of shallow river systems to further our understanding of intermittent river-groundwater connectivity. The method provides broad coverage over multiple spatial scales and is inexpensive to deploy. This investigation showed that the parameter of electrical resistivity is sensitive to hydrogeological parameters that are important for understanding the seasonality of connected and disconnected waters. This work also highlights that the connectivity along this portion of the Rio Grande occurs in a short time period. This spatiotemporal assessment supports sustainable conjunctive river water management practices that require substantial understanding of interactions between surface and groundwater for long-term solutions to issues of water quality and quantity, especially within a changing global environment of hydrology.

REFERENCES

Acworth, R., Dasey, G., 2003. Mapping of the hyporheic zone around a tidal creek using a combination of borehole logging, borehole electrical tomography, and cross-creek electrical imaging, New South Wales, Australia. *Hydrogeology Journal*, 11:3:368–377.

Archie, G.E., 1942. The electrical resistivity log as an aid in determining some reservoir characteristics, *Transactions of the American Institute of Mining, Metallurgical, and Petroleum Engineers*, 146:54-62.

Banks, E.W., Simmons, C.T., Love, A.J., Shand, P., 2011. Assessing spatial and temporal connectivity between surface water and groundwater in a regional catchment: Implications for regional scale water quantity and quality. *Journal of Hydrology*, 404:30-49.

Brunner, P., Cook, P.G., Simmons, C.T., 2011. Disconnected surface water and groundwater: From theory to practice. *Ground Water*, 49:460-467.

Brunner, P., Simmons, C.T., Cook, P.G., 2009. Spatial and temporal aspects of the transition from connection to disconnection between rivers, lakes and groundwater. *Journal of Hydrology*, 376:159–169.

Brunner, P., Therrien, R., Renard, P., Simmons, C.T., Franssen, H.-J.H., 2017. Advances in understanding river-groundwater interactions. *Reviews of Geophysics*, 55:818–854.

Clémence, H., Marc, P., Véronique, D., Toihir, A., 2017. Monitoring an artificial tracer test within streambed sediments with time lapse underwater 3D ERT. *Journal of Applied Geophysics*, 139:158-169.

Cubbage, B., Noonan, G.E., Rucker, D.F., 2017. A modified Wenner array for efficient use of eight-channel resistivity meters. *Pure and Applied Geophysics*, 174:2705–2718.

Crook, N., Binley, A., Knight, R., Robinson, D.A., Zarnetske, J., Haggerty, R., 2008. Electrical resistivity imaging of the architecture of substream sediments. *Water Resources Research*, 44:W00D13.

deGroot-Hedlin, C., Constable, S.C., 1990. Occam's inversion to generate smooth, two-dimensional models from magnetotelluric data. *Geophysics*, 55:1613–1624.

Elephant Butte Irrigation District. EBID Main Website. (n.d.). https://www.ebid-nm.org/

Findlay, S., 1995. Importance of surface-subsurface exchange in stream ecosystems: The hyporheic zone. *Limnology and Oceanography*, 40:159–164.

Fuchs, E.H., King, J.P., Carroll, K.C., 2019. Quantifying disconnection of groundwater from managed-ephemeral surface water during drought and conjunctive agricultural use. *Water Resources Research*, 55:5871-5890.

Harvey, J.W., Gooseff, M.N., 2015. River corridor science: Hydrologic exchange and ecological consequences from bedforms to basins. *Water Resources Research*, 51:6893–6922.

Humberson, D.G., 2021. Sediment texture and grain size analyses results from Rio Grande at Mesquite, NM. Personal Communication, January 19, 2021.

Ikard, S., Teeple, A., Humberson, D., 2021. Gradient self-potential logging in the Rio Grande to identify gaining and losing reaches across the Mesilla Valley. *Water*, 13:1331.

Irvine, D.J., Brunner, P., Hendricks Franssen, H.-J., Simmons, C.T., 2012. Heterogeneous or homogeneous? Implications of simplifying heterogeneous streambeds in models of losing streams. *Journal of Hydrology*, 424–425:16–23.

Johnson, T.C., Slater, L.D., Ntarlagiannis, D., Day-Lewis, F.D., Elwaseif, M., 2012. Monitoring groundwater-surface water interaction using time-series and time-frequency analysis of transient three-dimensional electrical resistivity changes. *Water Resources Research*, 48:W07506, doi:10.1029/2012WR011893.

King, W.E., Hawley, J.W., Taylor, A.M., Wilson, R.P., 1971. Geology and ground-water resources of central and western Doña Ana County, New Mexico. New Mexico Bureau of Mines and Mineral Resources Hydrologic Report, No. 1, 64 p.

Krause, S., Hannah, D.M., Fleckenstein, J.H., Heppell, C.M., Kaeser, D., Pickup, R., Pinay, G., Robertson, A.L., Wood, P.J., 2011. Inter-disciplinary perspectives on processes in the hyporheic zone. *Ecohydrology*, 4:481– 499.

Loke M.H., Acworth I., Dahlin, T., 2003. A comparison of smooth and blocky inversion methods in 2D electrical imaging surveys. *Exploration Geophysics*, 34:182–187.

Loke, M.H., Chambers, J.E., Rucker, D.F., Kuras, O., Wilkinson, P.B., 2013. Recent developments in the direct-current geoelectrical imaging method. *Journal of Applied Geophysics*, 95:135-156.

Mansoor, N., Slater, L., 2007. Aquatic electrical resistivity imaging of shallow-water wetlands. *Geophysics*, 72:F211–F221.

McLachlan, P.J., Chambers, J.E., Uhlemann, S.S., Binley, A., 2017. Geophysical characterisation of the groundwater–surface water interface. *Advances in Water Resources*, 109:302-319.

Nickerson, L., 1986. Selected geohydrologic data for the Mesilla Basin, Doña Ana County, New Mexico, and El Paso County, Texas. U.S. Geological Survey Open-File Report 86-75. US Geological Survey.

Ntarlagiannis, D., Robinson, J., Soupios, P., Slater, L., 2016. Field-scale electrical geophysics over an olive oil mill waste deposition site: evaluating the information content of resistivity versus induced polarization (IP) images for delineating the spatial extent of organic contamination. *J. Appl Geophys*, 135:418–426.

Nyquist, J., Freyer, P., Toran, L., 2008. Stream bottom resistivity tomography to map ground water discharge. *Ground Water*, 46:561–569.

Rucker, D., 2010. Moisture estimation within a mine heap: An application of cokriging with assay data and electrical resistivity. *Geophysics*, 75:1:B11-B23.

Sasaki, Y., 1992. Resolution of resistivity tomography inferred from numerical Simulation. *Geophysical Prospecting*, 40:453–463.

Shabaga, J.A., Hill, A.R., 2010. Groundwater-fed surface flow path hydrodynamics and nitrate removal in three riparian zones in southern Ontario, Canada. *Journal of Hydrology*, 388: 52-64.

Shukla, M.K., 2013. *Soil physics: An introduction*. Baca Raton, FL: CRC Press.

Singha, K., Pidlisecky, A., Day-Lewis, F.D., Gooseff, M.N., 2008. Electrical characterization of non-Fickian transport in groundwater and hyporheic systems. *Water Resources Research*, 44:W00D07.

Sophocleous, M., 2002. Interactions between groundwater and surface water: The state of the science. *Hydrogeology Journal*, 10:52–67.

Stummer, P., Maurer, H., Green, A.G., 2004. Experimental design: Electrical resistivity data sets that provide optimum subsurface information. *Geophysics*, 69:1:120-139.

Teeple, A.P., 2017. Geophysics and geochemistry-based assessment of the geochemical characteristics and groundwater-flow system of the U.S. part of the Mesilla Basin/Conejos-Médanos aquifer system in Doña Ana County, New Mexico, and El Paso county, Texas, 2010-12. U.S. Geological Survey Scientific Investigations Report 2017-5028, 183p.

USIBWC, 2014. Flood control improvements to the Rio Grande canalization project in Vado, New Mexico: Supplemental Environmental Assessment (SEA), United States Section, International Boundary and Water Commission (USIBWC), 45p.

van Genuchten, M.Th., Leij, F.J., Yates, S.R., 1991. The RETC Code for Quantifying the Hydraulic Functions of Unsaturated Soils, Version 1.0. EPA Report 600/2-91/065, U.S. Salinity Laboratory, USDA-ARS, Riverside, California.

Ward, A.S., Gooseff, M.N., Singha, K., 2010. Imaging hyporheic zone solute transport using electrical resistivity. *Hydrological Processes: An International Journal*, 24:948-953.

Ward, A.S., 2016. The evolution and state of interdisciplinary hyporheic research. Wiley Interdiscip Rev, *Water*, 83-103.

Winter, T.C., Harvey, J.W., Franke, O.L., Alley, W.M., 1998. Ground water and surface water, a single resource. USGS Circular 1139, 79p.

Wroblicky, G.J., Campana, M.E., Valett, H.M., Dahm, C.N., 1998. Seasonal variation in surface-subsurface water exchange and lateral hyporheic area of two stream-aquifer systems. *Water Resources Research*, 34:317-328.

Zhou, S., Yuan, X., Peng, S., Yue, J., Wang, X., Liu, H., Williams, D.D., 2014. Groundwater-surface water interactions in the hyporheic zone under climate change scenarios. *Environmental Science and Pollution Research*, 21:13943-13955.

APPENDIX

Figure 19 supports a homogeneous site analysis and the resulting van Genuchten parameters are typical of a sand.

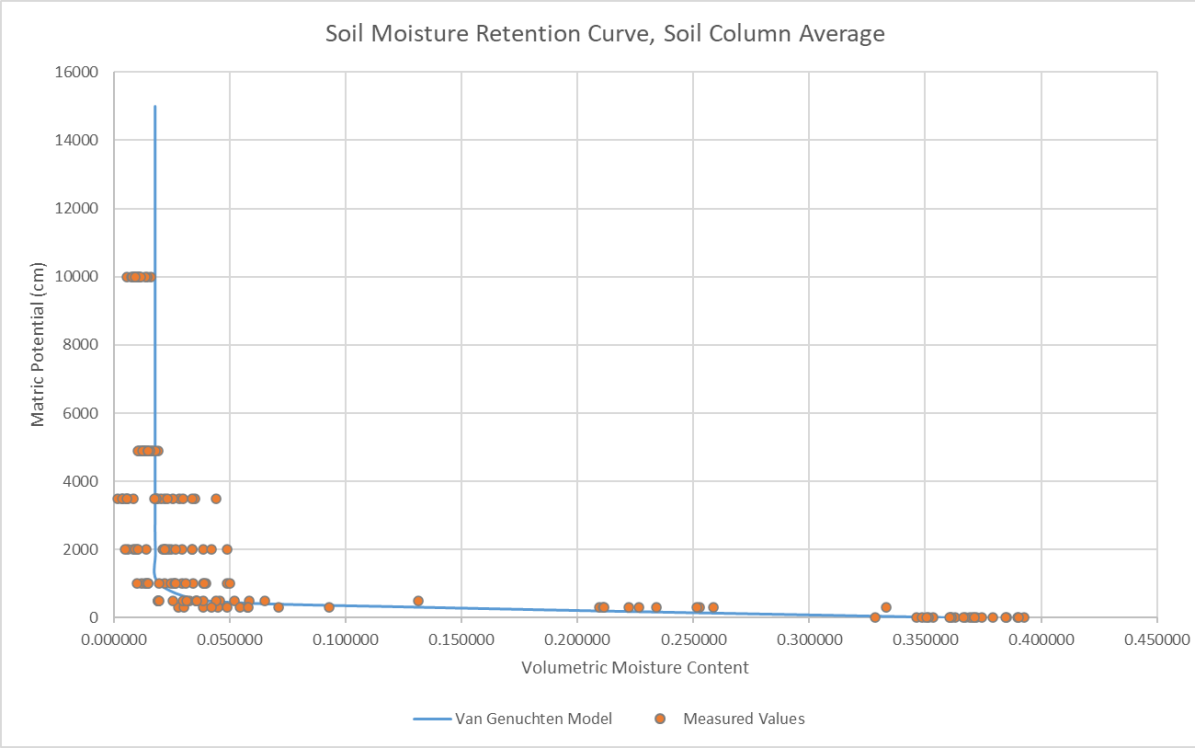

Figure 19. Unsaturated hydraulic conductivity curve of Rio Grande alluvium.

Figure 20 delineates that the average bulk conductivity has a slight positive correlation with the pore water conductivity, which aligns with empirical theory, though currently the magnitude of this correlation for these specific site soils has been quantified.

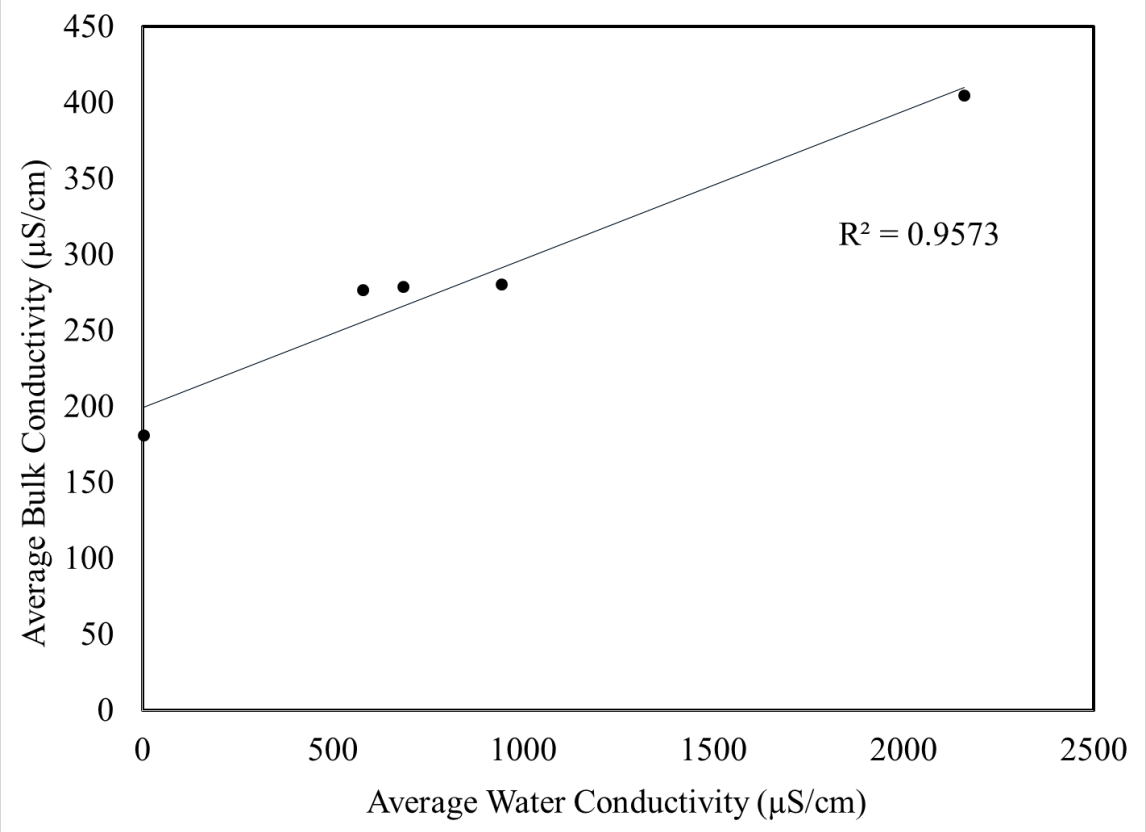

Figure 20. Average bulk conductivity vs. average pore water conductivity at water saturation 0.75 in Rio Grande alluvium.

In order to calculate the dispersivity of the Rio Grande alluvium, a soil tracer column experiment was performed. The result is a breakthrough curve for a sample of field site soil (Figure 21) fitted to a CXTFIT model for when a fluid without the tracer is injected into a fully saturated soil column at a constant flow rate, followed by a known concentration of tracer (in this case, Pentafluorobenzoic acid or PFBA) for a number of pore volumes (here, 2.62 PV), and then back to the non-tracer fluid. Samples of the water discharged through the soil were collected every minute for 30 seconds. These samples were then analyzed with a UV-Vos spectrophotometer for their absorption of the "fingerprint" wavelength at 254 nm that PFBA emits. This absorption was directly converted to a concentration in mg/L. The results indicate only slight dispersion within the Mesquite site soils.

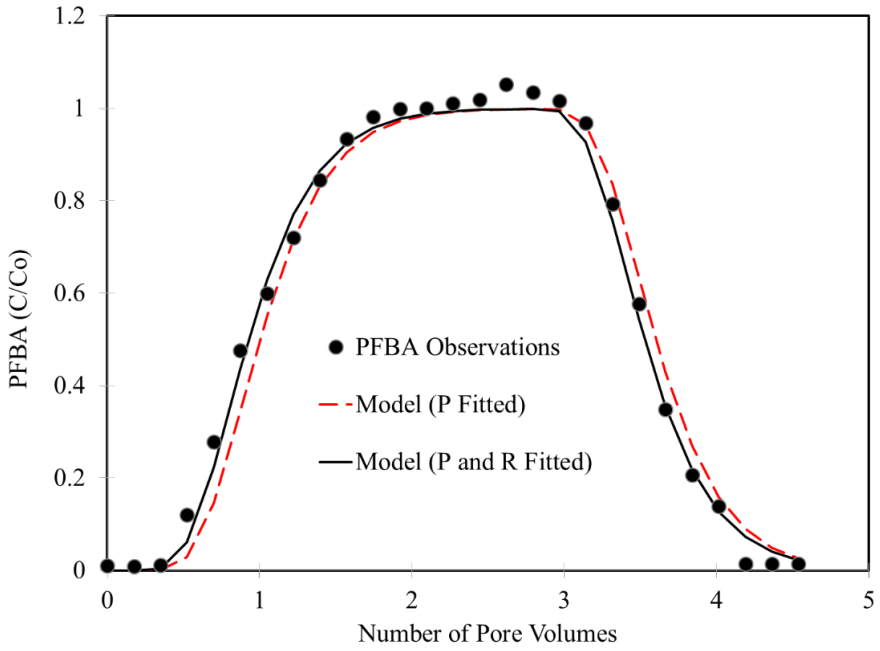

Figure 21. The breakthrough curve of Rio Grande alluvium, where C/Co is the ratio of detected concentration PFBA to the injected concentration, and PV is the number of pore volumes.

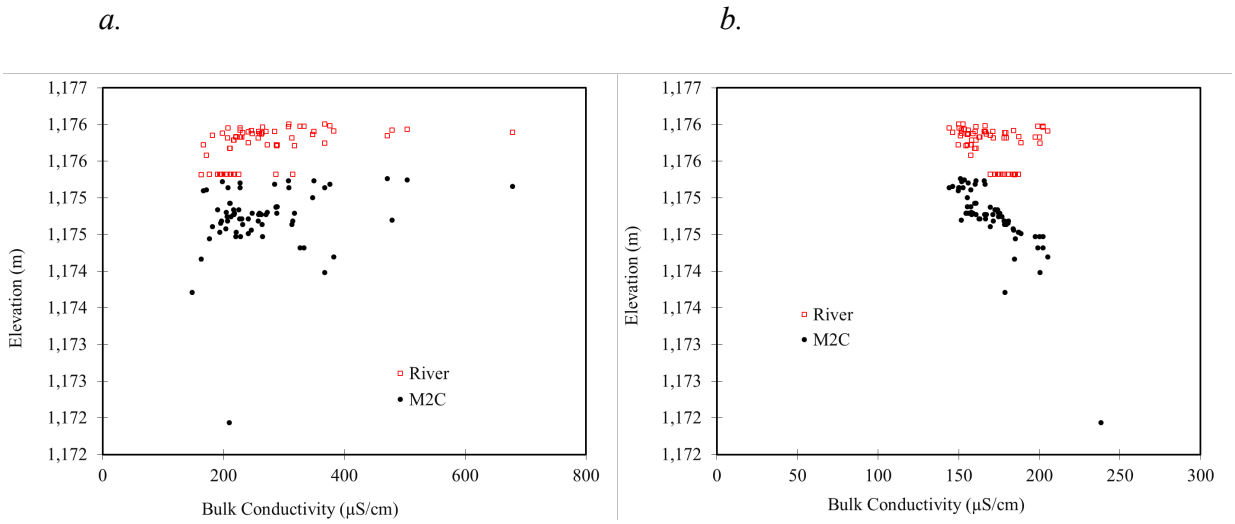

Figure 22. Shallow (a) ERT bulk conductivity and deep (b) ERT bulk conductivity vs. elevations of both river and groundwater.

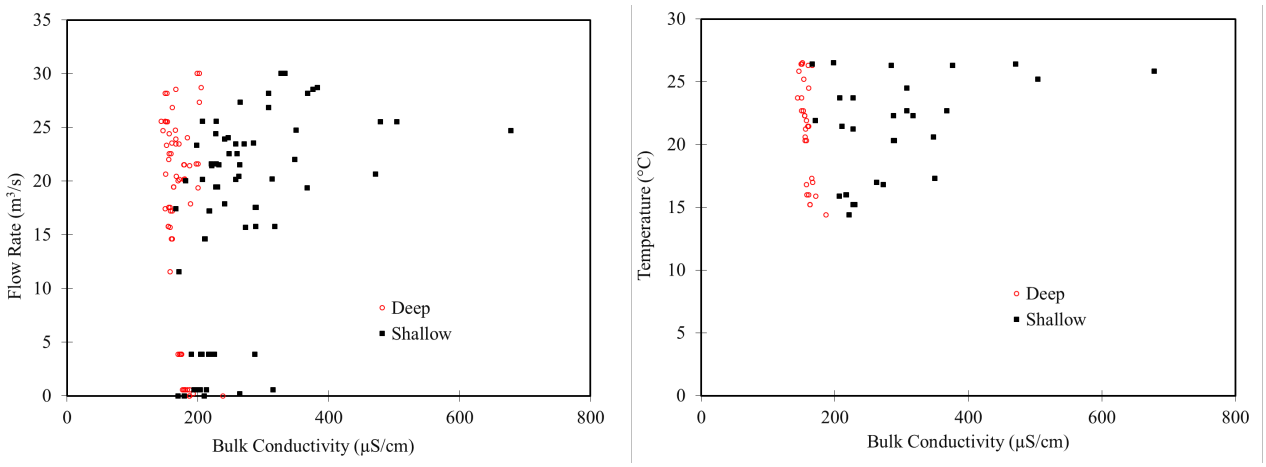

Figure 23. Deep and Shallow ERT bulk conductivities vs. river flow rate (top) and aqueous river temperature (bottom).

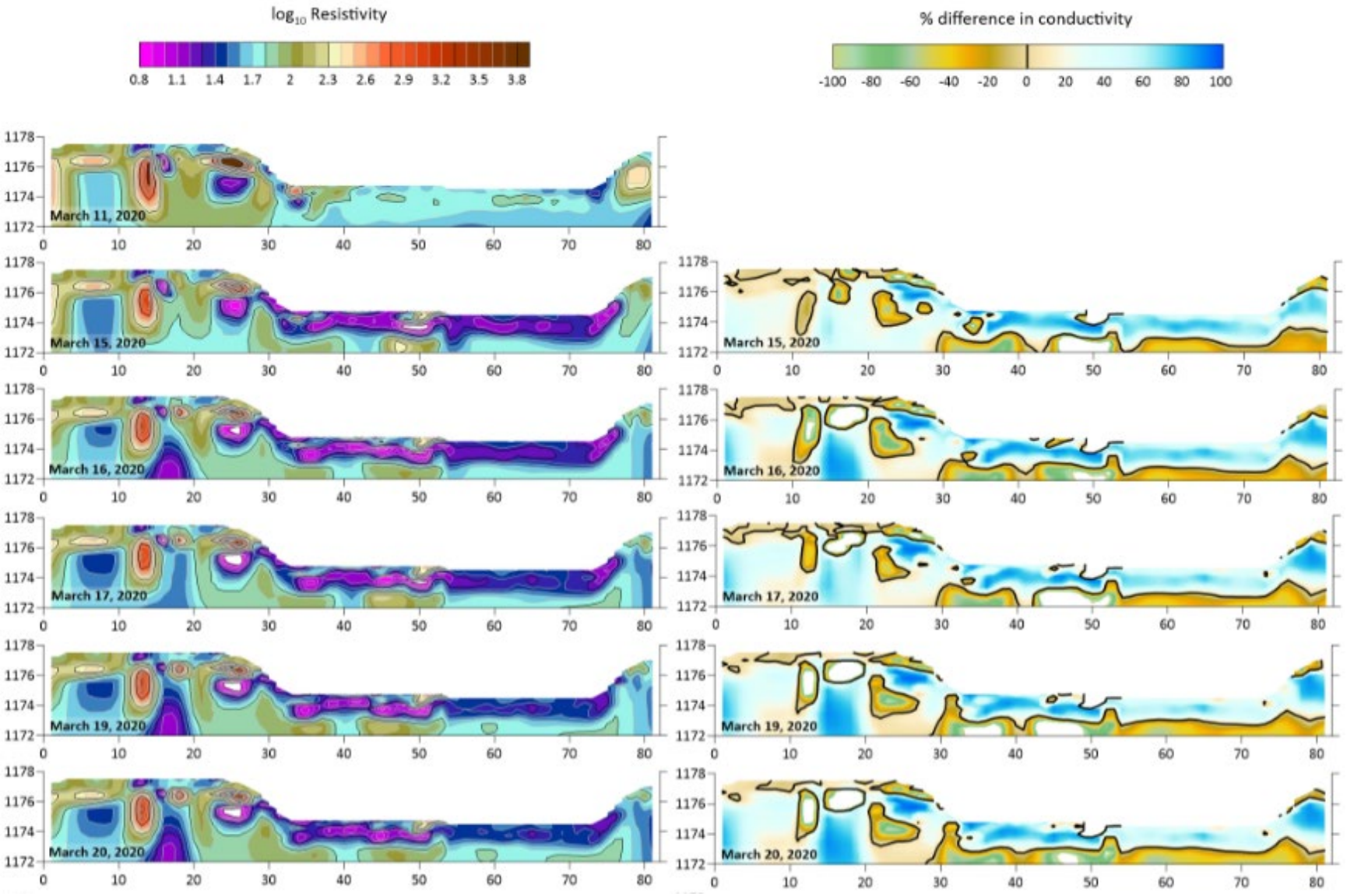
log10 Resistivity
0.8 1.1 1.4 1.7 2 2.3 2.6 2.9 3.2 3.5 3.8
% difference in conductivity
-100 -80 -60 -40 -20 0 20 40 60 80 100
March 11, 2020
March 15, 2020
March 16, 2020
March 17, 2020
March 19, 2020
March 20, 2020
1178
1176
1174
1172
0 10 20 30 40 50 60 70 80

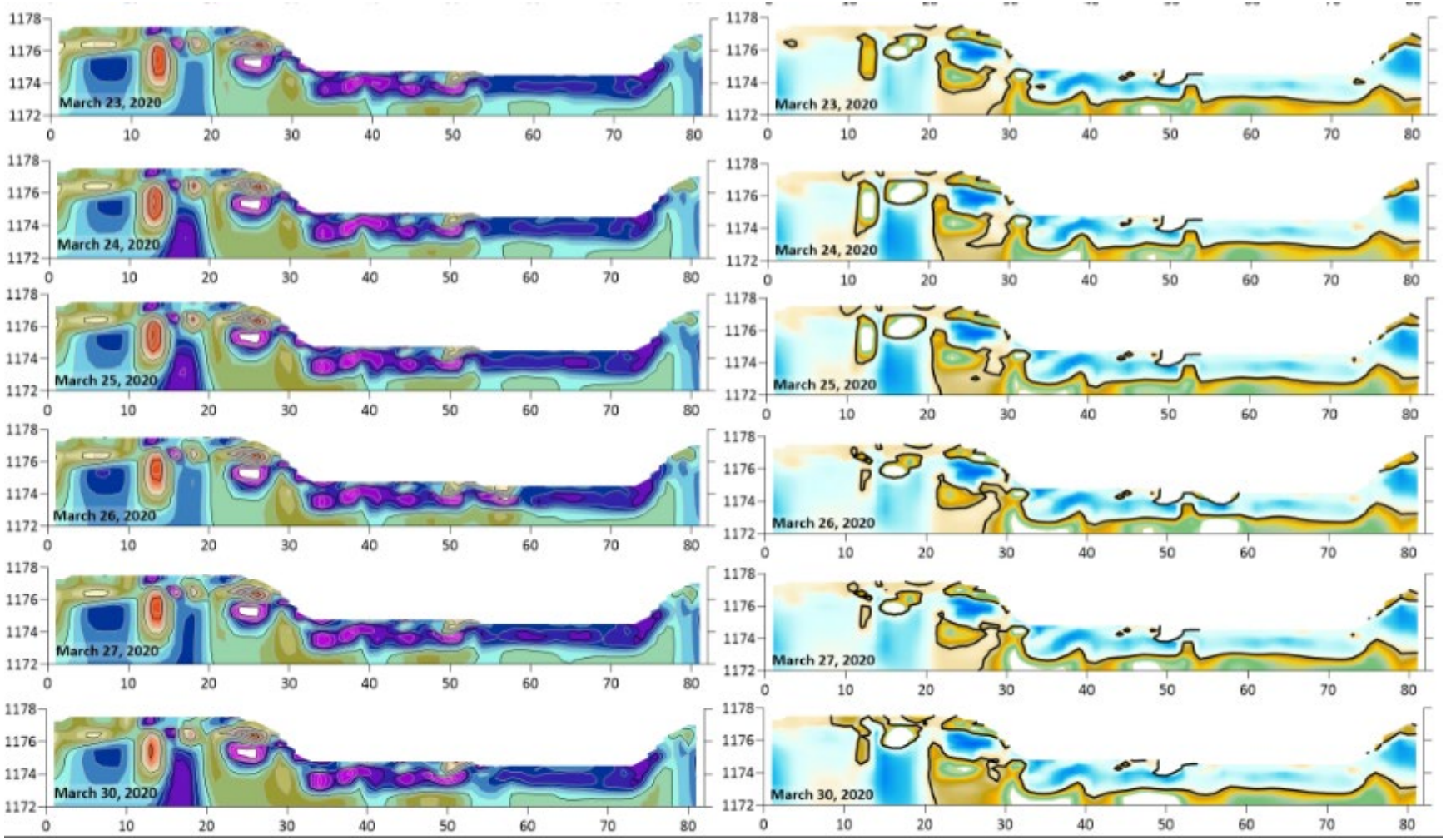
March 23, 2020
March 24, 2020
March 25, 2020
March 26, 2020
March 27, 2020
March 30, 2020
1178
1176
1174
1172
0
10
20
30
40
50
60
70
80

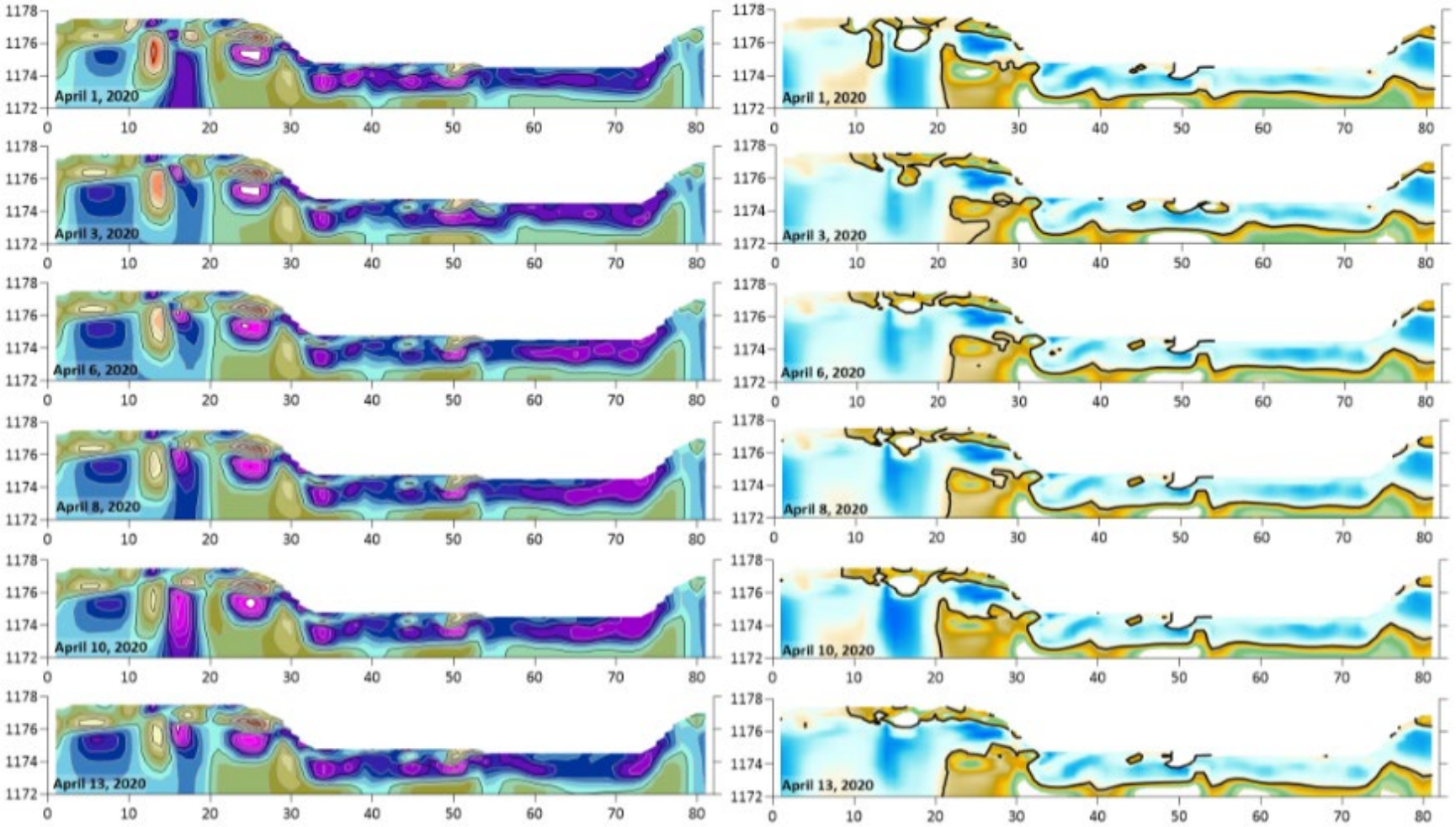
April 1, 2020
April 3, 2020
April 6, 2020
April 8, 2020
April 10, 2020
April 13, 2020
1178
1176
1174
1172
0
10
20
30
40
50
60
70
80

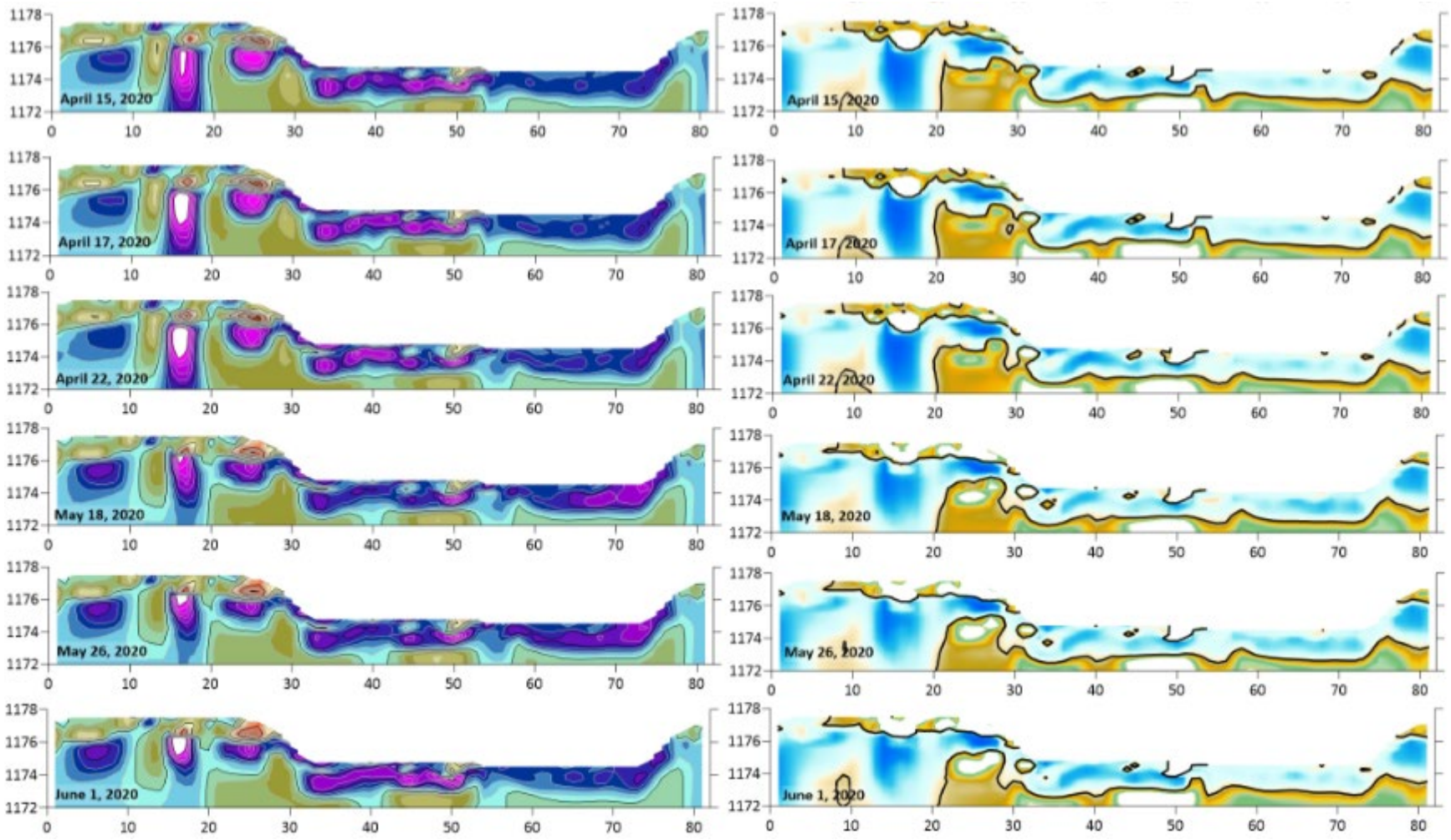
April 15, 2020
April 17, 2020
April 22, 2020
May 18, 2020
May 26, 2020
June 1, 2020
1178
1176
1174
1172
0
10
20
30
40
50
60
70
80

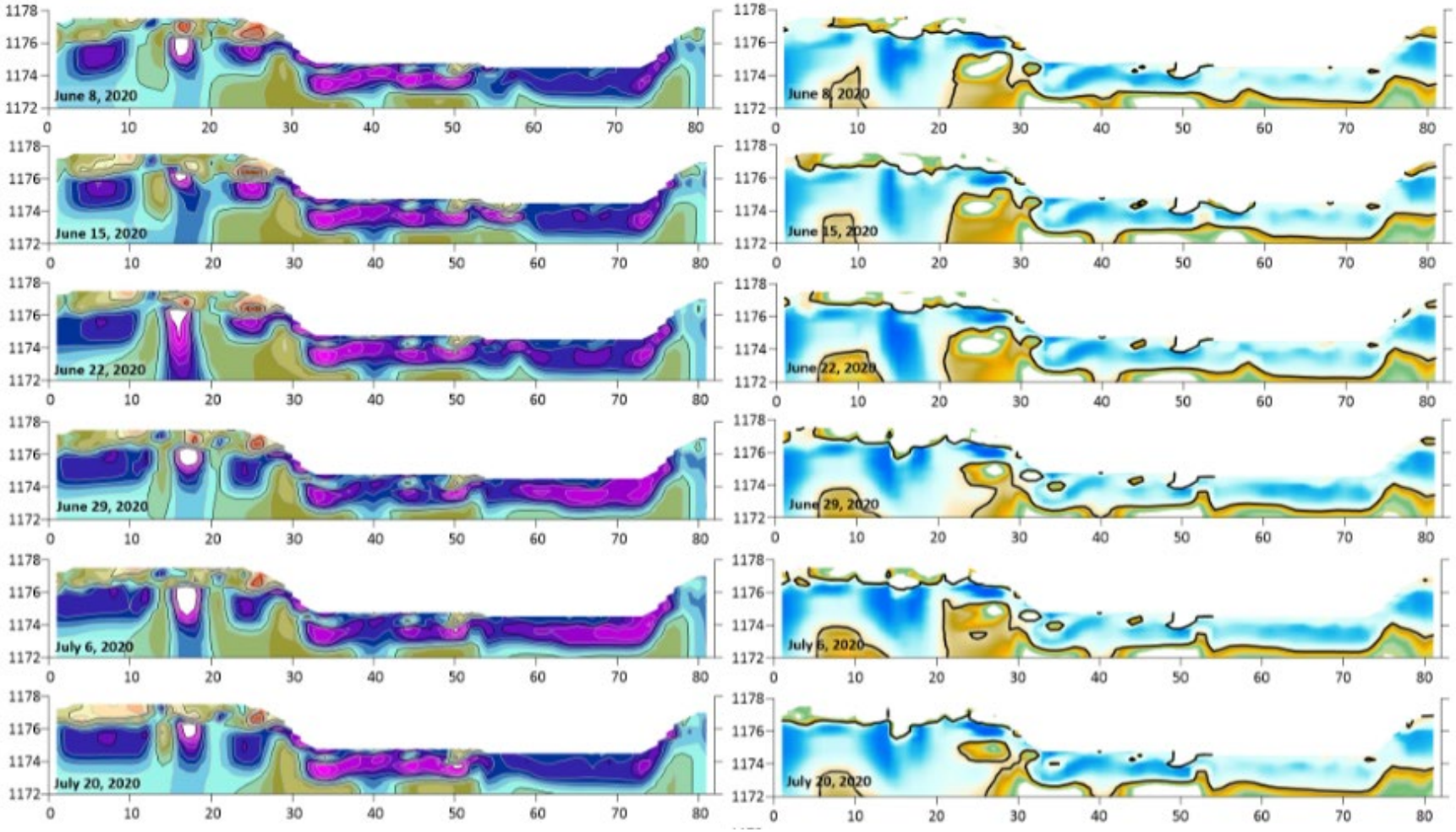
June 8, 2020
June 15, 2020
June 22, 2020
June 29, 2020
July 6, 2020
July 20, 2020
1178
1176
1174
1172
0
10
20
30
40
50
60
70
80

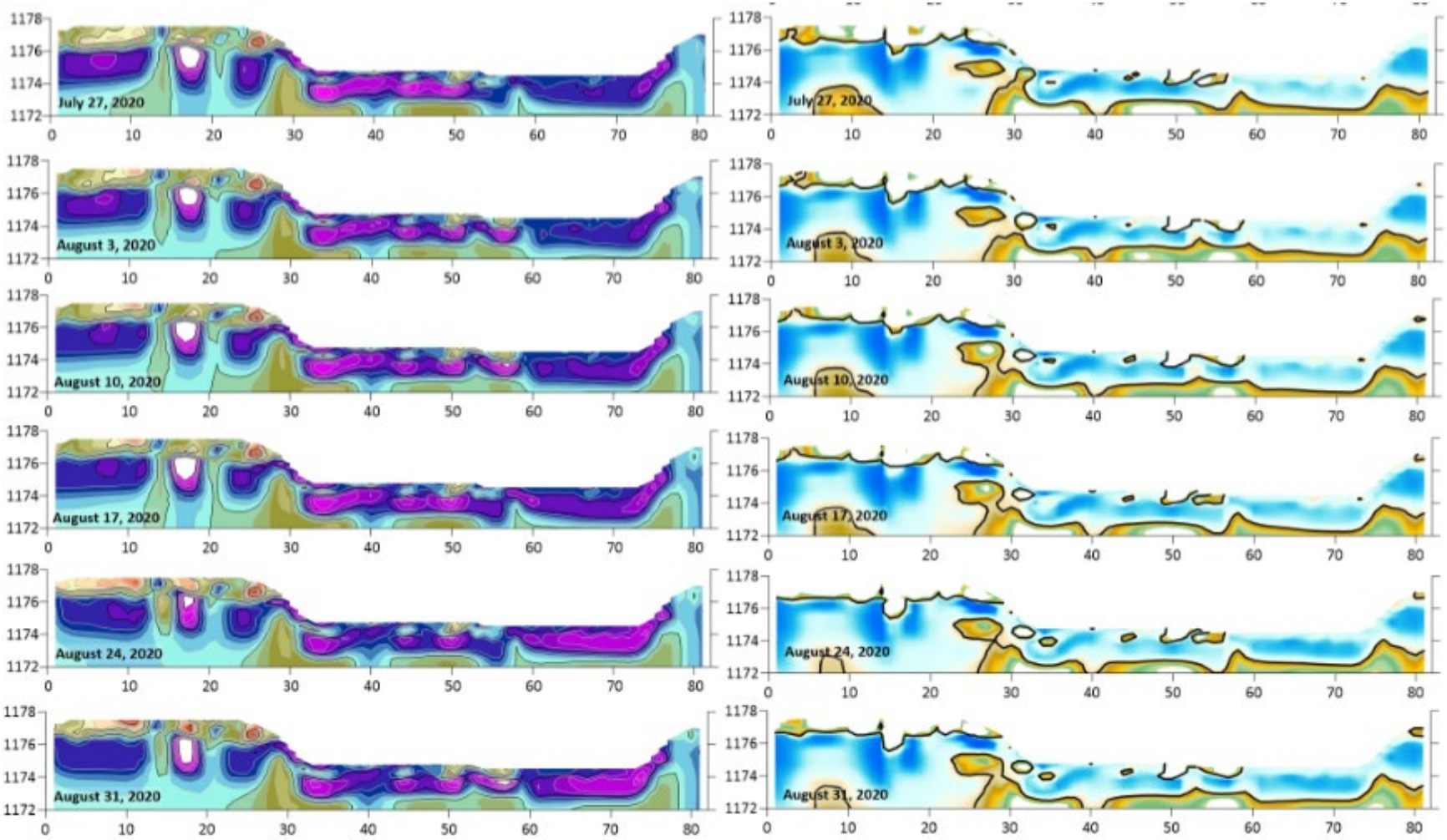
July 27, 2020
August 3, 2020
August 10, 2020
August 17, 2020
August 24, 2020
August 31, 2020
1178
1176
1174
1172
0
10
20
30
40
50
60
70
80

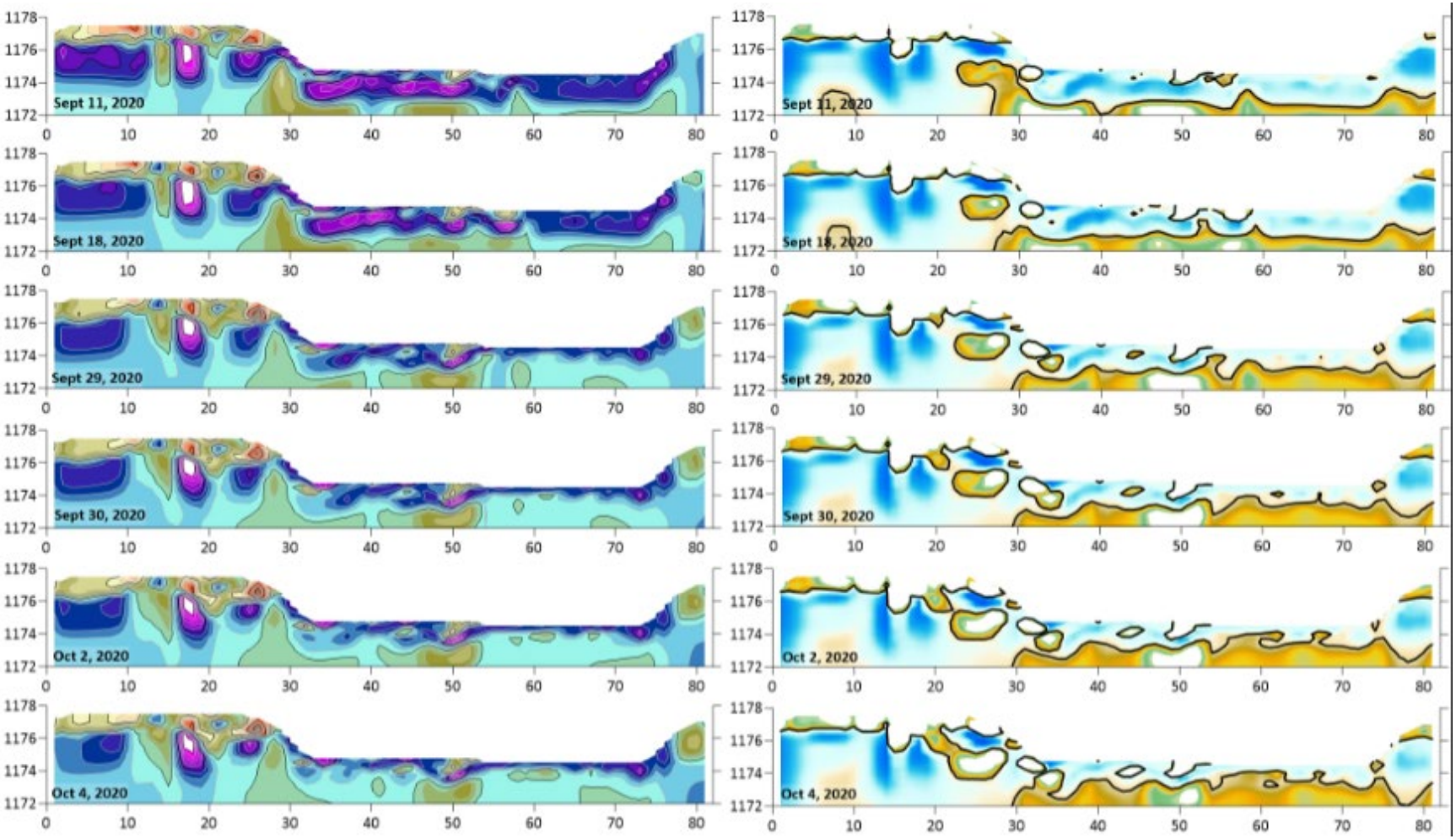
Sept 11, 2020
Sept 18, 2020
Sept 29, 2020
Sept 30, 2020
Oct 2, 2020
Oct 4, 2020
1178
1176
1174
1172
0
10
20
30
40
50
60
70
80

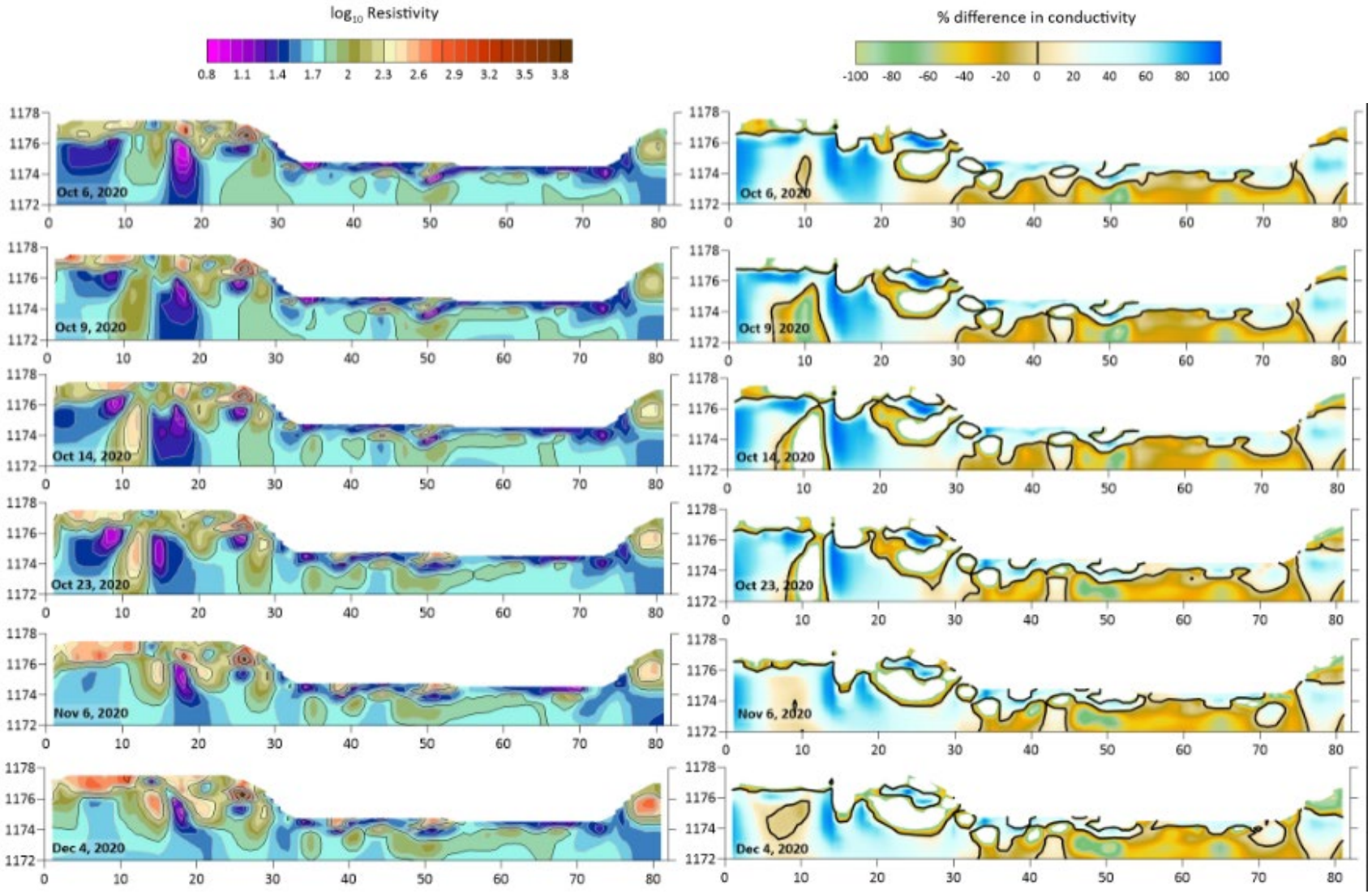

Figure 24. All resistivity snapshots (meters amsl over distance in meters) throughout the 2020 irrigation season.

Table 3. Variables for calculating hydraulic conductivity of Rio Grande alluvium using both constant and falling head methods.

	Run	Δh (cm)	V (mL)	t (s)	Q (ml/s)	A (Δh/Δl) (cm^2)	K (cm/s)
Constant Head Run 1	1	33	137	180	0.76111	53.3091	1.43E-02
	2	30	64	180	0.35556	48.4629	7.34E-03
	3	26	60	180	0.33333	42.0011	7.94E-03
Falling Head Run 1	1	33	-	-	-	-	-
	2	30	90	226.59	1.1	0.09531	7.36E-03
	3	26	95	239	1.15385	0.1431	1.05E-02
	4	22	100	352	1.18182	0.16705	8.31E-03
Constant Head Run 2	1	33	102	180	0.56667	53.3091	1.06E-02
	2	30	42	180	0.23333	48.4629	4.81E-03
	3	26	30	185	0.16216	42.0011	3.86E-03
Falling Head Run 2	1	33	-	-	-	-	-
	2	30	122	387.27	1.1	0.09531	4.31E-03
	3	26	91	512.46	1.15385	0.1431	4.89E-03
	4	22	98	712.57	1.18182	0.16705	4.10E-03

where Δh= change in height, V= volume, t= time, Q= flow rate, A=area, and
K= hydraulic conductivity